GENERATION OF PHASE-LOCKED HIGH HARMONICS BY IMPLEMENTING AN OPTICAL FREQUENCY DIVIDER

NURUL SHEEDA BINTI SUHAIMI

A thesis submitted in partial fulfillment
of the requirements for the degree of
Doctor of Philosophy (Engineering)

To

Department of Engineering Science
Graduate School of Informatics and Engineering
University of Electro–Communications
Tokyo, Japan

March 2016

GENERATION OF PHASE-LOCKED HIGH HARMONICS BY IMPLEMENTING AN OPTICAL FREQUENCY DIVIDER

NURUL SHEEDA BINTI SUHAIMI

Approved by:

Chair of Committee:
Prof. Masayuki Katsuragawa, Advisor
Department of Engineering Science _____
University of Electro–Communications

Committee Members:
Prof. Ken'ichi Nakagawa
Department of Engineering Science _____
University of Electro–Communications

Prof. Kaoru Minoshima
Department of Engineering Science _____
University of Electro–Communications

Assoc. Prof. Toru Morishita
Department of Engineering Science _____
University of Electro–Communications

Assoc. Prof. Ryosuke Shimizu
Department of Engineering Science _____
University of Electro–Communications

Dedicated to

my husband

Muhamad Khairul Abdullah

and my parents

Suhaimi Muslim

& Nasimah Mohd. Abbas

和文概要

光周波数領域における周波数分周の技術は光周波数標準の確立を目指す大きな流れの一部として独立したレーザーをコヒーレントにリンクすることを目的として研究されてきた。周波数分周で生成された光は等間隔の周波数間隔を持つ位相同期されたモードを形成し，その周波数比は整数比となる。位相同期されたモードはその位相を操作することにより高繰り返しレートを持つ超短パルス光を含む任意の光電場波形ができる。近年, パルスレーザーを用いた実験においては 125THz と非常に高い繰り返しレートを持つ波形整形が達成されている。しかしながら，連続波（CW）領域ではこのような高繰り返しレートを持つ波形整形はまだ達成されていない。これは適切な CW 光源がまだ開発されていないからである。

本博士論文では CW における超高繰り返し超短パルスの生成および任意波形整形を目標として、光周波数分周を用いて位相同期した $1f:2f:3f$ の周波数比を持つ光源を生成し，さらにそこから非線形光学素子を用いた和周波発生（SFG）によって高次のモード（周波数 $1f+3f=4f$, $2f+3f=5f$）を生成した。結果として 5 本の位相同期されたモードが達成された。ここで生成されたモードの間隔は 125THz（繰り返し時間間隔 8fsec）に及ぶ。CW 領域でこのような超高繰り返しレートを持つ超短パルス光生成・任意波形光整形は達成されておらず，本研究で生成した光源を用いることでこれが可能となる。また、1 モードあたりのパワーが大きいことから 1 モードを単独で取り出して高周波数精度を持つ波長可変な単一波長レーザーとして使用することも可能となる。

ABSTRACT

We have successfully generated a new broadband coherent light source in the continuous wave (CW) regime which is an ensemble of multi-harmonic radiations including the fundamental frequency by implementing a frequency dividing technology. The frequency dividing technology which divides an optical frequency to an integer ratio has been studied with the aim of coherently linking independent lasers as part of a historical trend toward the establishment of an optical frequency standard. Such lasers are attractive not only for establishing a frequency standard but also as a coherent light source itself for various practical uses. The laser radiations produced with such technology has provided us five phase-locked harmonics with extremely wide frequency spacing and bandwidth that extends from 124.7 to 623.7 THz, f_1: 2403 nm (36 mW), f_2: 1201 nm (371 mW), f_3: 801 nm (26 mW), f_4: 600 nm (28 mW), f_5: 480 nm (4 mW). Each harmonic shows a good beam quality, practical spectral power and fine phase coherence among them both in time and space. The system is uniquely designed that all harmonics are generated and propagate coaxially which has not been demonstrated by anyone yet. This design gives the advantage of robustly maintaining the phase coherence among the harmonics against disturbances. The potential applications for this light source can be diverse. In the frequency domain, each of the harmonics can be used as a single-frequency laser source. Moreover, by locking the system to a frequency standard, they can be used for ultra-high precision technology such as high resolution spectroscopy and high precision frequency metrology. In the time domain, the broadband spectrum can be used to synthesize ultrashort pulses train which can be very useful in the study of ultrafast science and technology. The highlight is that this light source has a high potential for the arbitrary optical waveform (AOW) synthesis in the continuous wave (CW) regime. The arbitrary-shaped optical field wave in the time scale of sub-femtosecond can be synthesized by precise control of the spectral phase and amplitude of a broadband harmonics. Such waves can be used to control the motion of electron through atoms and molecules which can be very useful for atto-science study. This technology has not been performed yet due to the limitation of the existing CW light source.

In this thesis, we demonstrated that the frequency of 801-nm (f_3) single-frequency diode laser is exactly divided by three by generating the difference frequency with another single-frequency diode laser at wavelength of 1201nm

(f_2~2/3f_3), producing a radiation at wavelength of 2403 nm (f_1=f_3–f_2). Then, we generated the second harmonic of f_1, (f_2'=2f_1) and compared it with the frequency f_2 of 1201-nm laser. Based on such frequency comparison, we controlled the 1201-nm laser so that the two frequencies, f_2 and f_2', coincide exactly. When this frequency control is achieved with a phase precision, the optical-frequency divide-by-three process is completed, resulting in generation of three phase-locked harmonics with an exact integer-frequency ratio of f_1 : f_2 : f_3 = 1 : 2 : 3. Then, based on the generated three phase-locked harmonics, we further generated the 4th (f_4: 600 nm) and the 5th (f_5: 480 nm) phase-locked harmonics by generating sum frequencies among the three phase-locked radiations, as f_4 = f_1 + f_3 and f_5 = f_2 + f_3. The total of five harmonics was evaluated in terms of phase coherence stability, spectral power and beam quality.

ACKNOWLEDGMENTS

I would like to use this opportunity to express my sincere gratitude to all the talented and generous people who have guided and supported me on the long journey to finish my Ph.D research in UEC. I have been extremely privileged to work with them and truly, without their support, my accomplishments would never be possible.

My supervisor, Prof. Masayuki Katsuragawa, has devoted invaluable amounts of time, attention, and support in guiding me through my Ph.D. research. His guidance and advice were very critical in helping me to become a good researcher. Working for him has been a wonderful experience.

I also appreciate Prof. Ken'ichi Nakagawa, Prof. Kaoru Minoshima, Assoc. Prof. Toru Morishita and Assoc. Prof. Ryosuke Shimizu for their valuable advices and comments in helping me to upgrade my work.

My research and my student's life had been very enjoyable from working with many wonderful people in Katsuragawa Laboratory. I have to thank Dr. Yoshii Kazumichi and Dr. Chiaki Ohae, who have taught me a great deal of lab skills. I am also glad to have known and worked with Gavara Trivikramarao, who has been such a good colleague and a great friend since my first year in UEC. Of course I won't forget the help and fun that I have from the other members of Katsuragawa Lab.

Finally, I want to thank my parents and my husband for their deep understanding and endless support. I dedicate this dissertation to them with much love.

Table of Contents

List of Figures

List of Tables

Chapter 1

Introduction

1.1 Literature review and motivations

The development of laser light performance has become the key to many extreme and advance technologies, not only in optical science but in the field of chemistry, biology and others as well. One of the most exciting developments is that of ultrashort laser pulses with a time-scale of a few femtoseconds (10^{-15} sec) [1] which open doors for us to interact with matters in the atomic world. The ultrashort laser pulses can be used to control the excitation of states in atoms and molecules [2, 3] where we can study the progression and intermediate states of chemical reactions. In recent years, the developments of ultrashort laser pulses have further advanced towards the time scale of attosecond (10^{-18} sec), which opens the possibility to probe the properties of even smaller and lighter matter than the atom, such as the electrons [4]. The opposite performance of isolated pulses is a continuous train of optical pulses, and the generation of laser pulses with ultra-high repetition rate of terahertz (10^{12} Hz) has already been demonstrated [5]. If the technical difficulties can be overcome, the ultra-high repetition rate laser pulses have the potential to be applied for ultra-high speed optical communication, which is currently limited to

several hundreds of gigahertz (10^9 Hz). The establishment of ultra-high precision single frequency laser with the precision transferred from an optical frequency standard opens the door to perform high precision frequency metrology [6], high resolution laser spectroscopy [7] and laser cooling [8]. Another extreme laser source that are developing rapidly are the short wavelength lasers in the vacuum ultraviolet (VUV) and the extreme ultraviolet (XUV) region [9]. Such laser sources are already massively used in the lithography of advanced microelectronic circuits and the medical procedures (such as photorefractive keratectomy), and they are also expected to find more applications in the areas of atomic physics, photochemistry, photobiology and high resolution spectroscopy. Another extreme light source is the super-intense laser where each of the light pulse is produced with a power of more than a terawatt (10^{12} watts). Such intense laser can interact with gas to generate higher harmonics more than 200 times the fundamental laser frequency – into the X-ray range [10], which could be a source for biological imaging. Furthermore, the interaction of the super intense laser with plasmas (known as laser plasma) can be

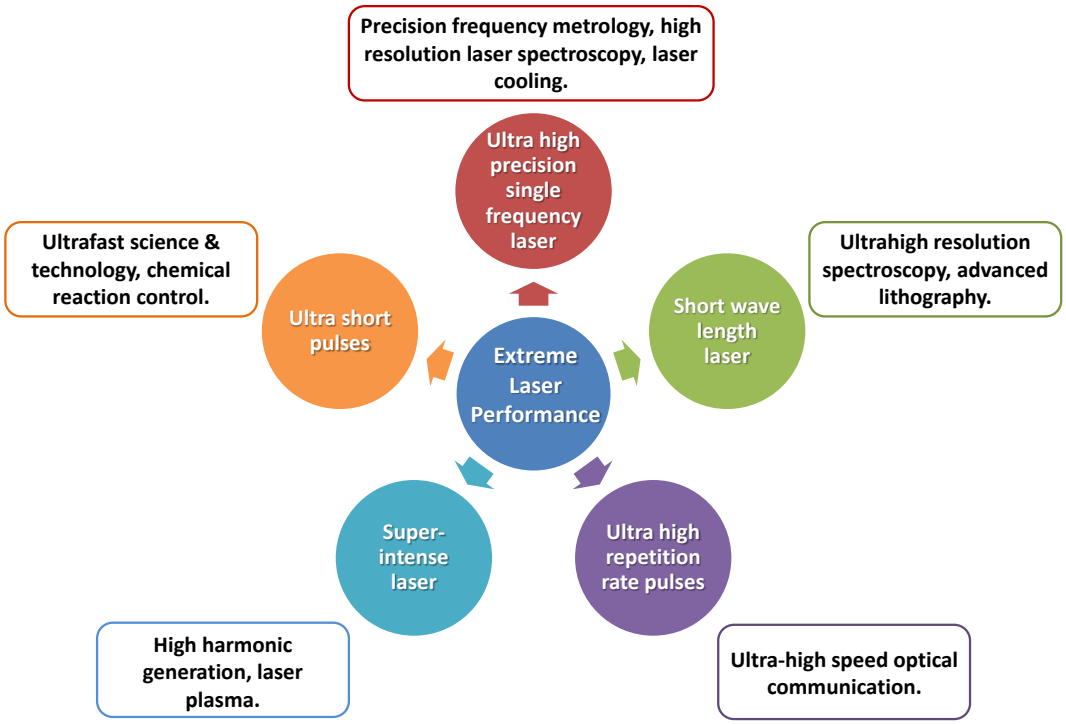

Fig. 1.1: Extreme laser performances and the potential applications that could be stimulated by it.

used to accelerate subatomic particles such as electrons which can be useful for wide applications, including proton therapy for cancer treatment, material characterization, detection of dangerous substances such as explosives, and high-energy particle physics [11]. These extreme performances of laser light source and their potential applications are illustrated in Fig. 1.1.

Until today, research for a new type of laser source is still actively ongoing by targeting more advance laser performances. One of the most high impact inventions of a laser light source is the optical frequency comb which was first demonstrated by Hansch group in the late 70 ' s using picosecond lasers [12] and have attracted even more attention since Roy. J. Glauber, John L. Hall and Theodor W. Hansch were awarded the Nobel Prize in Physics in 2005 for the great invention. A frequency comb is a broadband coherent light source consists of evenly spaced frequency components. This broadband light source in frequency domain is equivalent to ultrashort pulses in time domain which is connected through Fourier transform theory (as shown in Fig. 1.2). Therefore, the frequency comb can perform as high precision single frequency laser in the frequency domain and also as ultrashort laser pulses in the time domain.

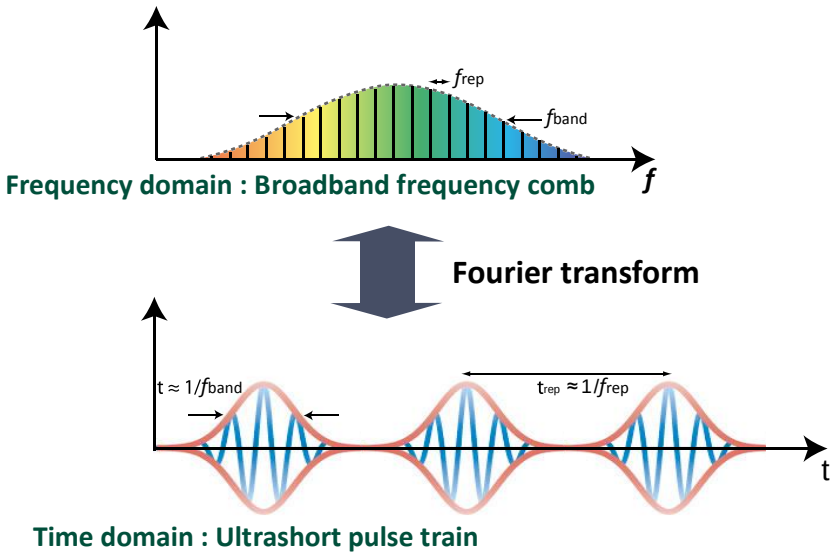

Fig. 1.2: The connection of a broadband frequency comb (top) and a train of ultrashort pulses in time domain (bottom) through Fourier transformation. Here, f_{rep}: frequency spacing, f_{band}: comb bandwidth, t_{rep}: repetition rate and t: pulse width.

The extended performance of the ultrashort laser pulses is the technology of "designing" the laser pulses. The term of "designing" indicates the control of the rapid electric field oscillations of the laser that determines the pulse shape through manipulation of the phase and amplitude of the frequency components. The pulse designing technology is known as pulse shaping and has been developed over recent years [13]. This technology allows us to generate user-defined time-domain intensity waveforms which are shaped envelopes that contain many cycles of rapidly oscillating optical field. These waveforms are also referred to as arbitrary optical waveforms (AOW). The potential applications of AOW are much more diverse, including study of atomic motion, coherent control of chemical reactions,

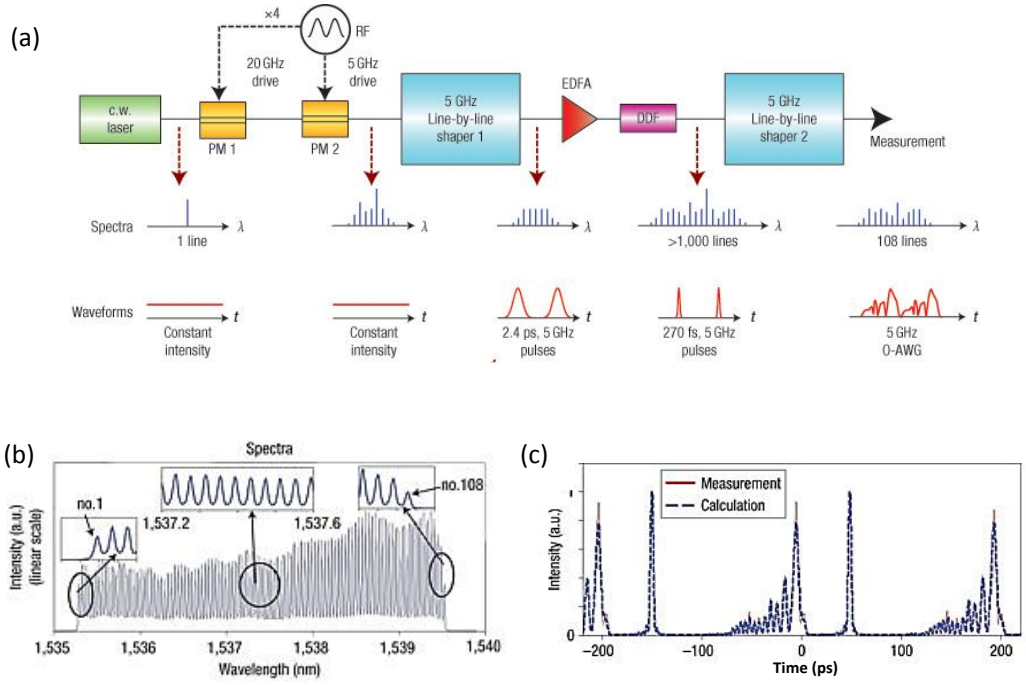

Fig. 1.3: Complex shaped optical waveform synthesis using more than 100spectral comb lines. (a) Schematic of high-rate ultrashort pulse generation experiment. (b) Spectrum of selected 108 spectral lines. (c) Intensity correlation of selected lines that shows an example of AOW with a very complex waveform. [Courtesy from *Nat. Photon. 1, 463 (2007)*].

frequency selective nonlinear microscopy and imaging [14] and light wave communications [15]. *Weiner et al.* [16] has demonstrated the generation of complex shaped optical waveforms by line-by-line pulse shaping technique, as shown in Fig. 1.3. They employed the method of CW laser modulation that generated over 1000 frequency lines with 5 GHz frequency spacing to be used as the light source. The generated envelope waveforms are in picosecond time scale due to the frequency spacing of 5 GHz.

Another interesting challenge that has attracted much attention in the optical physics field is to produce instantaneous optical light fields in the shapes that are similar to those obtains by the function generators in the RF region, such as square, saw tooth, triangular and sub-sine and cosine waveforms, instead of complex shaped enveloped. Based on the Fourier transform theory, such periodic waveforms can be synthesized by an appropriate superposition of harmonics sine or cosine waves starting from the fundamental frequency. In order to synthesize the target waveforms, first, the frequencies of the coherent light source need to span more than one octave [17]. Secondly, the initial phases of the frequency components including the phase relationship among them must be stable to allow precise control over the phase and amplitude for the purpose of temporal pulse shaping. There are several potential approaches that have been developed to generate light source that could satisfy the requirements above. One of the approaches is by phase-locked two individual mode-locked femtosecond lasers to extend the coherent bandwidth [18]. However, the generated spectral lines are closely spaced which makes it difficult to perform individual phase and amplitude control. An approach that can overcome this limitation is by molecular modulation [19-23], which uses the excitations of vibrational or rotational transitions of molecules to modulate the driving lasers and generate a comb of spectrum that span more than one octave. The generated frequency comb has a very wide (several hundred of THz) and equal frequency spacing where each spectral component can be used and manipulated individually to produced AOW. In a very recent years, *Chan. et al* [24] has successfully demonstrated the generation of AOW based on the optical light field by manipulating the phase and amplitude of five harmonic waves obtained from the coherent modulation of hydrogen molecule (as shown in Fig. 1.4) which is a huge step in realizing the idea of AOW generator.

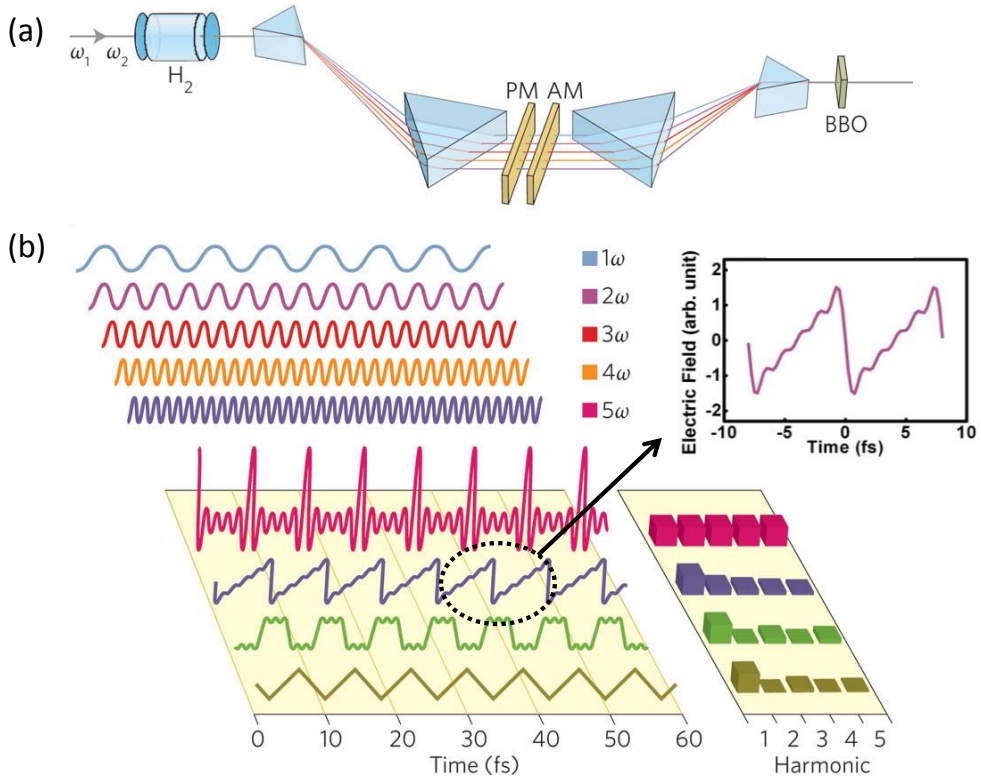

Fig. 1.4:.(a) Schematic of the experimental setup to synthesize waveforms using harmonics generated by coherent modulation of the H_2 molecule. AM and PM are liquid crystal spatial light modulators (LCSLMs) that, respectively, attenuate the powers (and thus amplitudes) of the harmonics and adjust and compensate their phases. (b) Pictorial demonstration of ultrafast waveforms obtained by the coherent superposition of the first five harmonics of a fundamental wavelength. The five harmonic waves are depicted above, the waveforms below. The panel on the lower right depicts the spectral field amplitudes required for the synthesis of the respective waveforms on the left. The 8.02-fs pulse spacing originates from a fundamental wavelength of 2406 nm. [Courtesy from *Science* ***331****, 1165 (2011)*].

A further step of improvement that can be made is to extend this technique to the CW regime by using CW laser source. CW laser source could make the synthesized waveforms inherently more stable. There are already several groups that have made progress towards developing CW coherent light sources. One approach is by using CW-stimulated Raman scattering in a high-finesse cavity [25] which

successfully generated three spectral components with bandwidth span from 0.8 to 3.2 μm. Another approach is by using a CW-pumped optical parametric oscillator based on cascading quadratic nonlinearities [26] which has successfully produced a 4 THz wide CW frequency comb. A generation of broadband CW multi-harmonics with spectral bandwidth of ~470 THz by employing a frequency division-by-three optical parametric oscillator was recently demonstrated by *A. H. Kung* group [27]. However, the frequency fluctuation is quite large due to the linewidth of the pump laser and the phase coherence of the multi-harmonics is not clarified. Another possible approach to produce a broadband CW multi-harmonics comb is by nonlinear mixing of phase-coherent laser sources, as proposed by *T. W. Hansch* [17] but the system is very complex for realization. However, recently, *Chiodo et al.* employed an almost similar concept and demonstrated a phase locking of two independent lasers at 1544 (Er-doped fiber laser) and 1029 nm (Yb-doped fiber laser) by matching the third harmonic of the 1544 nm radiation with the second harmonic of the 1029 nm radiation, which resulted in the phase-locked multi-frequency radiations ($2f_c$:1544 nm, $3f_c$:1029 nm, $4f_c$:772 nm, and $6f_c$:515 nm) [28].

The purpose of this study is to develop a new light source in the CW regime which is not only applicable for the AOW generations, but also has the potential to be used for various applications. The target light source can be expected to have these five criteria: (1) Broad bandwidth, (2) Composed of integer multiplied high harmonics including the fundamental frequency, (3) High phase coherence, (4) Extremely wide frequency spacing and (5) Practical spectral power. Our approach is by using the concept proposed by *T. W. Hansch* [17] but the system is designed to allow all the harmonics to be generated and propagate coaxially to robustly maintain the phase coherence from disturbance. Therefore, the generated harmonics could be expected to have high phase-coherence in space and time. To my knowledge, such approach has not yet been performed by anyone. The phase-locking is performed by implementing a divide-by-three optical frequency division technique [29-33]. This technique allows lasers with large frequency gap to be connected and phase-locked based on nonlinear process, which will also results in three phase-locked harmonics including the two lasers. Higher harmonics are generated by the sum-frequency mixing of the three phase-locked harmonics. Furthermore, the massive development of highly efficient nonlinear crystal [34] has brought this technique to become more attractive as it allows high harmonics to be generated with high spectral power.

This new light source can be expected to have many potential applications. For examples, individually, the spectrums of the light source could be used as a high accuracy tunable single frequency laser by locking the system to a frequency standard for application of high precision metrology. As a whole, they can be used to generate ultrashort pulses for ultrafast technology studies. Furthermore, they can be expected to be applicable for the generation of AOW in the CW regime which has not yet been performed. This could be the key technology to open many more studies in the quantum control field.

1.3 Thesis context and overview

This thesis is divided into four major parts. First part is the concept of operation involved in the generation of high harmonics. Second part demonstrates the experimental techniques (master laser stabilization, divide-by-three optical frequency divider, high harmonics generation and spectral phase measurement) to generate five phase-locked harmonics and evaluate the phase stability among them. The results are presented and discussed in the third part. As conclusions, the achievements in this thesis are summarized together with discussions on the limitations. Finally, the future prospects of this study are briefly discussed. The details are described by chapter as follows.

In **chapter 2**, the concept on how to perform divide-by-three optical frequency division to generate the initial three phase-locked harmonics and then used them in nonlinear frequency mixing processes to produce the 4^{th} and the 5^{th} harmonics are explained. The principles of Pound-Drever-Hall technique which is used to frequency stabilized the master laser in the experimental setup is also explained in details. Finally, the concept of spectral interference is chosen to clarify the phase relationship among the generated five harmonics.

In **chapter 3**, the details of the experimental setup are explained. The experimental setup is divided into three main parts; stabilization of master laser, divide-by-three optical frequency divider and the high harmonics generation. First, the master laser is stabilized to a reference cavity by Pound-Drever-Hall technique. Then, the radiation from the stabilized master laser is introduced into the divide-by-three optical frequency divider together with radiation from a divider laser to generate the first three phase-locked harmonics. These three phase-locked harmonics are introduced into two nonlinear crystals sequentially to produce two higher harmonics via sum-frequency generations which makes the total of generated harmonics becomes five. The harmonics generated through quasi-phase matched nonlinear process are mutually-coherent in nature thus all the harmonics can be expected to be phase coherent. However, in order to confirm this condition, an interference measurement among the harmonics is performed to evaluate the stability of the phase relationship among all the harmonics.

In **chapter 4**, the experimental results from the setup explained in chapter 3 are presented. First, the frequency stability of the master laser is measured. Then, the performance evaluations of the phase-locking via divide-by-three optical frequency divider are explained. The generated five phase-locked harmonics are evaluated in terms of beam quality and spectral power. The phase relation stability among them is observed to clarify the stability of their phase relationship.

In **chapter 5**, the achievements and limitations of this study are given.

Finally, in **chapter 6**, the future prospects of the achievement in this study are briefly discussed. This includes the further improvement and the potential applications.

References for Chapter 1:

1. J. DeMaria, C. Ferrar, and G. E. Danielson, "Self mode-locking of lasers with saturable absorbers", Jr., Appl. Phys. Letters 8, 22 (1966).
2. R. S. Judson and H. Rabitz, "Teaching lasers to control molecules", Phys. Rev. Lett. 68, 1500 (1992).
3. M. Shapiro, P. Brumer, "Principles of the quantum control of molecular processes", Rep. Prog. Phys. 66, 859 (2003).
4. G. Sansone, E. Benedetti, F. Calegari, C. Vozzi, L. Avaldi, R. Flammini, L. Poletto, P. Villoresi, C. Altucci, R. Velotta, S. Stagira, S. De Silvestri and M. Nisoli, "Isolated Single-Cycle Attosecond Pulses", Science 314, 443 (2006).
5. M. Katsuragawa, K. Yokoyama, T. Onose, and K. Misawa, "Generation of a 10.6-THz ultrahigh-repetition-rate train by synthesizing phase-coherent Raman-sidebands", Optics Express 13, 5628 (2005).
6. Th. Udem, R. Holzwarth & T. W. Hänsch, "Optical frequency metrology", Nature 416, 233 (2002).
7. R. Holzwarth, Th. Udem, T. W. Hänsch, J. C. Knight, W. J. Wadsworth, and P. St. J. Russell, "Optical Frequency Synthesizer for Precision Spectroscopy", Phys. Rev. Lett. 85, 2264 (2000).
8. C. S. Adams and E. Riis, "Laser cooling and trapping of neutral atoms", Prog. Quant. Elect. 21, 1 (1997).
9. C. Gohle, T. Udem, M. Herrmann, J. Rauschenberger, R. Holzwarth, H. A. Schuessler, F. Krausz and T. W. Hänsch, "A frequency comb in the extreme ultraviolet", Nature 436, 234 (2005).
10. Z. Chang, A. Rundquist, H. Wang, M. M. Murnane, and H. C. Kapteyn, "Generation of Coherent Soft X Rays at 2.7 nm Using High Harmonics", Phys. Rev. Lett. 79, 2967 (1997).
11. V. Malka, J. Faure, Y. A. Gauduel, E. Lefebvre, A. Rousse and K. T. Phuoc, "Principles and applications of compact laser–plasma accelerators", Nature Physics 4, 447 (2008).
12. J. N. Eckstein, A. I. Ferguson, T. W. Hänsch, C. A. Minard and C. K. Chan, "Production of deep blue tunable picosecond light pulses by synchronous pumping of a dye laser", Optics Communications 27, 466 (1978).
13. A. M. Weiner, "Femtosecond pulse shaping using spatial light modulators", Rev. Sci. Instrum. 71, 1929 (2000).
14. J. M. D. Cruz, I. Pastirk, M. Comstock, V. V. Lozovoy, and M.s Dantus, "Use of coherent control methods through scattering biological tissue to achieve functional imaging", Proc. Natl. Acad. Sci. 101 (2004).

15. J. D. McKinney, D. E. Leaird, and A. M. Weiner, "Millimeter-wave arbitrary waveform generation with a direct space-to-time pulse shaper", Opt. Lett. 27, 1345 (2002).
16. Z. Jiang, C. –B. Huang, D. E. Leaird and A. M. Weiner, "Optical arbitrary waveform processing of more than 100 spectral comb lines", Nat. Photon. 1, 463 (2007).
17. T.W. Hänsch, "A proposed sub-femtosecond pulse synthesizer using separate phase-locked laser oscillators", Opt. Commun., 80, 71 (1990).
18. R. K. Shelton, L. –S. Ma, H. C. Kapteyn, M. M. Murnane, J. L. Hall, J. Ye, "Phase-Coherent Optical Pulse Synthesis from Separate Femtosecond Lasers", Science 293, 1286 (2001).
19. S. E. Harris, A. V. Sokolov, "Subfemtosecond Pulse Generation by Molecular Modulation", Phys. Rev. Lett. 81, 2894 (1998)
20. A. Nazarkin et al, "Group-velocity-matched interactions in Hollow Waveguide", Phys. Rev. 65, 041802 (2002)
21. H. Kawano et al, "Generation of more than 40 rotational Raman lines by 336 picosecond and femtosecond Ti:sapphire laser for Fourier Synthesis", Appl. Phys. B Lasers Opt. 65, 1 (1997)
22. J. Q. Liang et al, "Sideband generation using strongly driven Raman coherence in solid hydrogen", Phys. Rev. Lett. 85, 2474 (2000)
23. T. Suzuki et al, "Octave-spanning Raman comb with carrier envelope offset control", Phys. Rev. Lett. 101, 243602 (2008)
24. H. –S. Chan et al, "Synthesis and Measurement of Ultrafast Waveforms from Five Discrete Optical Harmonics", Science **331**, 1165 (2011).
25. J. T. Green, J. J. Weber, and D. D. Yavuz, "Continuous-wave light modulation at molecular frequencies", Phys. Rev. A 82, 011805(R) (2010).
26. V. Ulvila, C. R. Phillips, L. Halonen, and M. Vainio, "Frequency comb generation by a continuous-wave-pumped optical parametric oscillator based on cascading quadratic nonlinearities", Opt. Lett. 38, 4281 (2013).
27. Y. –Y. Lin, P. –S. Wu, H. –R. Yang, J. –T. Shy and A. H. Kung, "Broadband Continuous-Wave Multi-Harmonic Optical Comb Based on a Frequency Division-by-Three Optical Parametric Oscillator", Appl. Sci., 4(4), 515 (2014).
28. N. Chiodo, F. Du-Burck, J. Hrabina, M. Lours, E. Chea and O. Acef, "Optical phase locking of two infrared CW lasers separated by 100 THz", Opt. Lett., 39, 2936 (2014).
29. A. Douillet, J.-J. Zondy, G. Santarelli, A. Makdissi, and A. Clairon, "A Phase-Locked Frequency Divide-by-3 Optical Parametric Oscillator", IEEE TRANSACTIONS ON INSTRUMENTATION AND MEASUREMENT, 50, (2001).
30. P. T. Nee and N. C. Wong, "Optical frequency division by 3 of 532 nm in periodically

poled lithium niobate with a double grating", Opt. Lett., 23, 46 (1998).

31. D. –H. Lee, M. E. Klein, J. –P. Meyn, R. Wallenstein, P. Groß, and K. –J. Boller, "Phase-coherent all-optical frequency division by three", Phys. Rev. A 67, 013808 (2003).
32. O. Pfister, M. Mürtz, J. S. Wells, L. Hollberg, and J. T. Murray, "Division by 3 of optical frequencies by use of difference-frequency generation in noncritically phase-matched RbTiOAsO4", Opt. Lett. 21, 1387 (1996).
33. J. E. Bernard, B. G. Whitford, and L. Marmet, "Phase-locked optical divide-by-3 system for visible radiation", Opt. Lett. 24, 98 (1999).
34. D. S. Hum and M. M. Fejer, "Quasi-phasematching", Comptes Rendus Physique **8**, 180 (2007).

Chapter 2

The concepts

2.1 Introduction

For the purpose of providing a framework to perform highly efficient experiments and to predict the upcoming results, the concepts and theories behind this study must be studied and analyzed. With deep understanding of the concepts and the theoretical background, it can be estimated under what conditions the harmonics can be generated and controlled efficiently and to clarify the limitations in the system for further improvements.

Therefore, in this chapter, the concept and study behind each operation are explained. There are two main operations to generate the five phase-locked harmonics; the divide-by-three optical frequency division and the high harmonics generation. First, I will explain the concept of divide-by-three optical frequency division which is implemented to generate the first three phase-locked harmonics. Then, I will describe the concept of high harmonics generation by implementing second-order nonlinear processes to generate another two higher harmonics. I will also describe the concept of frequency locking by using Pound-Drever-Hall technique which is applied to lock the master laser in the experiment. Finally, a

theoretical study on harmonics interference is presented which is used as reference in the experimental study to confirm the phase coherence among the five harmonics.

2.2 Divide-by-three optical frequency division

The purpose of the divide-by-three optical frequency division is to generate three phase-locked harmonics including the fundamental. In this section, we will describe the concept of this operation and also the principles of optical phase-lock loop that provides feedback signal to the laser source.

2.2.1 The concept of operation

Figure 2.1 shows the concept behind the divide-by-three optical-frequency divider in the experimental system. First, I employ two laser sources as master and divider lasers, whose oscillation frequencies are f_3 and f_2, respectively. Then, I produce the difference frequency radiation, $f_1 = f_3 - f_2$, in a difference frequency generation (DFG) process. Furthermore, the f_1 radiation is doubled in a second harmonic generation (SHG) process to produce f_2' radiation. Next, I detect the beat signal between the f_2' and f_2 radiations, where the oscillation frequencies of the two laser sources are adjusted in advance so that $f_2' \sim f_2$ is satisfied. Finally, I feedback the detected beat signal to the f_2 divider- or f_3 master-laser source to control their oscillation frequencies so that they exactly satisfy $f_2 = f_2'$. When this locking is stabilized with phase coherence between f_2 and f_2', the divide-by-three optical-frequency division is completed, which means that the three phase-locked harmonics, f_1, f_2 and f_3 are obtained at frequency ratio of 1 : 2 : 3.

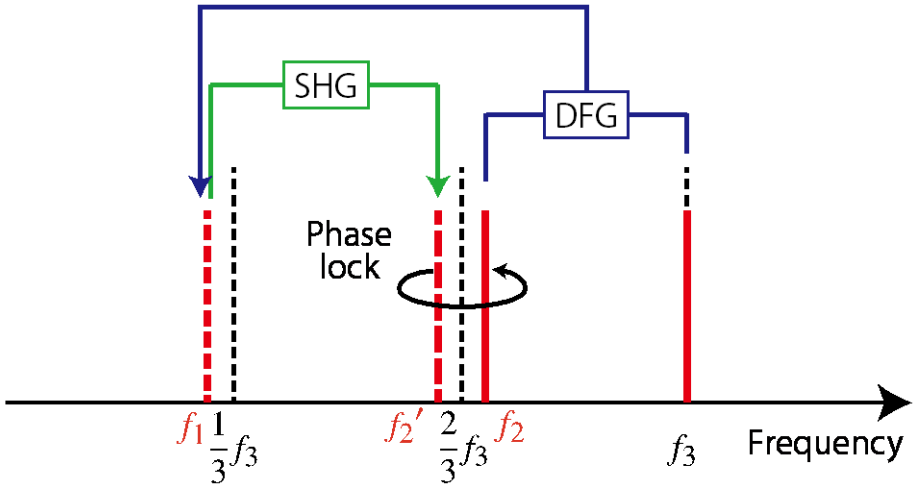

Fig. 2.1. Concept of a divide-by-three optical-frequency divider

2.2.2 Optical phase-lock loop

Basically, the performance of an optical frequency division is based on the efficiency of the phase-locking operation. Therefore, it is important to design an efficient feedback system to obtain high accuracy phase-locking. In this study, an optical phase-lock loop (OPLL) system is applied to perform the feedback process. This section describes the principles of operation of the OPLL.

Optical phase-locking scheme

The objective of an optical phase-lock loop (OPLL) is to have the divider (slave) laser tracing the frequency and the phase of the master laser. In the concept of divide-by-three optical frequency division, the master laser frequency is divided by three by DFG process with the divider laser. Then, the divider laser is phase-locked to the master laser by locking it to the second harmonic of the difference frequency between the slave and the master laser. The main elements of an optical phase-lock

loop are phase detector, loop filter and current controller that converts a voltage signal to current, as shown in Fig. 2.2. A local oscillator is used to produce a reference frequency for phase-locking the beat frequency that is generated by the lasers. The principles of the optical phase-lock loop operation are as follows. First, the beat signal from the optical frequency division process is detected by a high-speed photodetector. Then, the phase difference between the beat frequency and the reference frequency from the local oscillator is detected by the phase detector and is produced as a voltage signal. This voltage signal is sent through a loop filter and then is converted into current. This current is fed to the divider laser to control its oscillating frequency so that the phase difference between the beat frequency and the reference frequency becomes very close to zero.

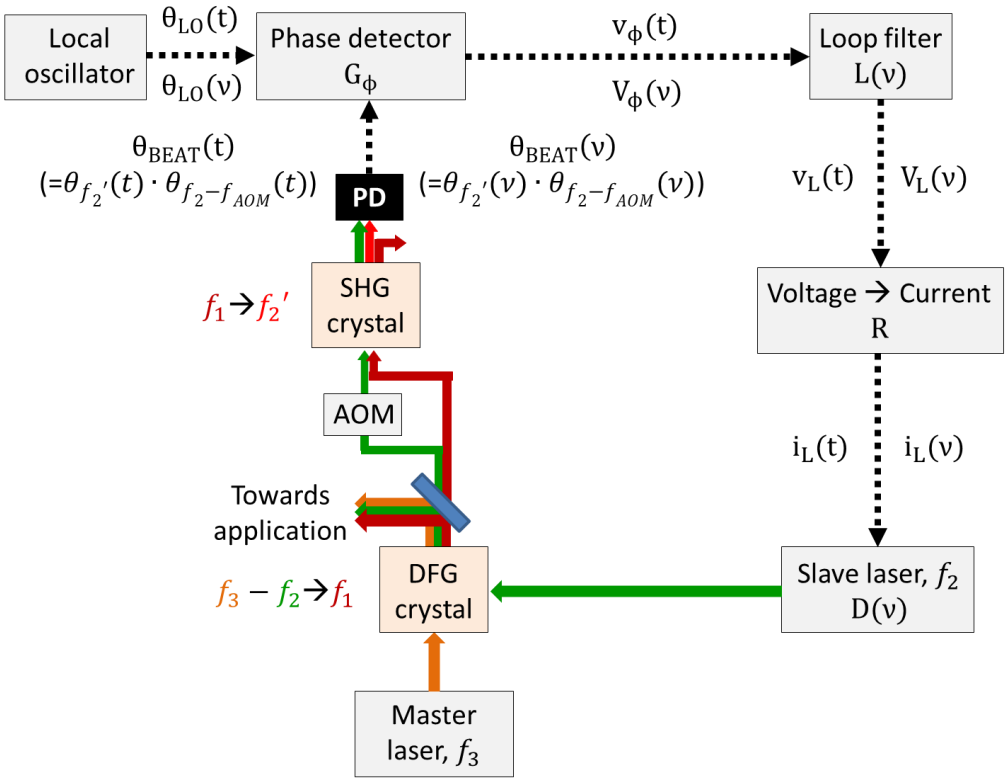

Fig.2.2 Block diagram of the phase-lock loop in optical frequency divider

Theory of optical phase-lock loop

It is convenient to use transfer functions to explain the feedback theory. The transfer function is treated as the variable of the Fourier frequency. In Fig. 2.2, **t** indicates the time variable; meanwhile, **ν** indicates the Fourier frequency variable.

The transfer functions in Fig. 2.2, $V_{\phi}(\nu)$, $V_{L}(\nu)$ and $I_{L}(\nu)$ are indicated as the following equations.

$$V_{\phi}(\nu) = G_{\phi}\{\theta_{LO}(\nu) - \theta_{BEAT}(\nu)\} = G_{\phi}\phi(\nu) \tag{2-1}$$

$$V_{L}(\nu) = V_{\phi}(\nu)L(\nu) \tag{2-2}$$

$$I_{L}(\nu) = \frac{V_{L}(\nu)}{R} \tag{2-3}$$

The phase difference between the two input signals from the phase detector is expressed by the following equation.

$$\phi(\nu) = \theta_{LO}(\nu) - \theta_{BEAT}(\nu) \tag{2-4}$$

Furthermore, small change of frequency in time is equal to the derivative of phase with respect to time.

$$\frac{d\theta_{BEAT}(t)}{dt} = \Delta f(t) \tag{2-5}$$

Fourier transfer of this equation is

$$i2\pi\upsilon\theta_{BEAT}(\nu) = \Delta F(\nu) \tag{2-6}$$

Transfer function of $\Delta F(\nu)$ is

$$\Delta F(\nu) = I_{L}(\nu)D(\nu) \tag{2-7}$$

From (2-6) and (2-7),

$$\theta_{BEAT}(\nu) = \frac{I_{L}(\nu)D(\nu)}{i2\pi\upsilon} \tag{2-8}$$

Therefore, from (2-1), (2-2), (2-3) and (2-8), the following transfer function is obtained.

$$\frac{\theta_{BEAT}(\nu)}{\theta_{LO}(\nu)} = H(\nu) = \frac{G_\phi L(\nu) D(\nu)}{i2\pi\upsilon R + G_\phi L(\nu) D(\nu)} = \frac{G(\nu)}{1 + G(\nu)} \tag{2-9}$$

Here, $H(\nu)$ is known as the closed-loop transfer function but I will not going to solve this function in this thesis. Instead, I will use the following function, which is known as the open-loop function, to estimate $H(\nu)$.

$$\mathrm{G}(\nu) = \frac{G_\phi L(\nu) D(\nu)}{i2\pi\upsilon R} \tag{2-10}$$

Transfer function of the loop elements

In order to determine the open loop function as mentioned above, it is important to know the properties of each element that involves in the current feedback process.

I. Phase detector : G_ϕ

A phase detector detects the phase different between two inputs and converts the information to a voltage signal. In this study, a digital phase detector is used where the voltage output is directly proportional to the detected phase difference. The proportionality constant is defined by G_ϕ with the unit of [V/rad].

II. ECDL frequency response towards current modulation: $D(\nu)$

Current flow in the ECDL changes the temperature, which leads to the change of cavity length inside the ECDL. The change of cavity length results in the change of oscillating frequency. However, the response of temperature change towards the current flow is limited to low frequency modulation. This means that the tuning of oscillating frequency depends on the current modulation range as well. When the current modulation reaches the frequency limit α, the tuning gain will decrease. The frequency – gain characteristics of $D(\nu)$ is defined as follows.

$$D(\nu) = G_d \frac{\alpha}{\mathbb{i}\nu + \alpha} \left[\frac{rad}{s}/V\right]$$

Here, G_d is the rate of ECDL frequency shift to current change. $\mathbb{i}\nu^{-1}$ is the coefficient of frequency to phase conversion.

III. Cable and optical path delay

Delay is the time for the error signal takes to go through one complete loop and this amount of time determines the limit of the loop bandwidth. The transfer function of delay is defined by the following equation,

$$\exp(-2\pi\mathbb{i}\nu\tau)$$

where τ is estimated from the length of light propagations and the cables.

IV. Loop filter：$L(\nu)$

There are two requirements need to be satisfied in the loop filter circuit. One is to compensate the phase delay that occurs at the current modulation limit α as mentioned above. The other requirement is to compensate the decrease of gain. In this study, the transfer function of the loop filter is estimated by using a circuit simulator (LT SPICE).

2.3 Nonlinear optical high harmonic generation

2.3.1 The concept of application

After I obtained the three phase-locked harmonics from the divide-by-three optical frequency division process, the second step is to expand the bandwidth of this light source by generating higher order harmonics. The important characteristics of the harmonics that need to be focused on in this operation are the phase coherence, the spectral power and the beam quality of the generated harmonics. These properties are important in order to widen the potential applications of this light source.

The chosen approach is to implement nonlinear optical process. Nonlinear optical process such as OPO, SHG, SFG and DFG has been a common approach for the purpose of generating coherent optical frequencies [1-3]. The features of this approach is that by placing a nonlinear medium in one or two reliably high power laser beams, higher harmonics can be generated. Furthermore, by employing a quasi-phase matched (QPM) based nonlinear medium, this approach can result in a compact system with high conversion efficiency. Also, the phase relation between the input light and the generated light is constant throughout the QPM nonlinear medium because of the phase-matching condition. Therefore, this approach satisfies the requirement for generating our target light source.

The concept of this approach is as follows. The three phase-locked modes from the frequency division system are introduced into two periodically-poled lithium niobate (PPLN) waveguides sequentially for SFG processes to generate the 4^{th} and 5^{th} harmonics as shown in Fig. 2.3. In order to maintain the phase coherence of the fundamental three modes and the generated two modes and from surrounding noises, all the modes are designed to propagate coaxially, which in my knowledge has never been performed yet.

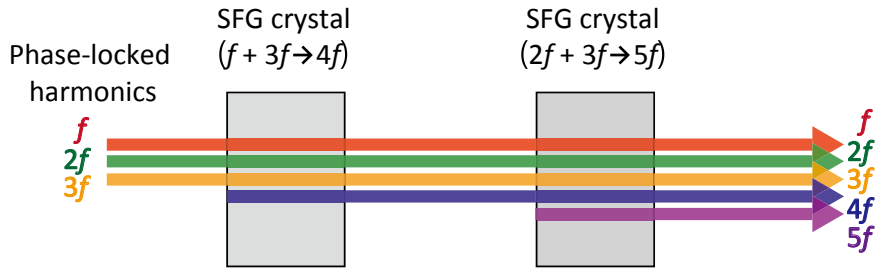

Fig. 2.3 Schematic of five harmonics generation based on sum frequency of three phase-locked modes from optical frequency divider.

In this section, the principles of second-order nonlinear optical process and nonlinear medium PPLN waveguide are explained.

2.3.2 Second-order nonlinear optical process

Second-order nonlinear optical process is also known as "three-wave mixing" because it involves the mixing of three electromagnetic waves, f_1, f_2, and f_3, (f_1< f_2 < f_3) where the magnitude of nonlinear response of the crystal is characterized by the $\chi^{(2)}$ coefficient. The common nonlinear effects that utilize the $\chi^{(2)}$ properties of the crystal are second-harmonic generation (SHG), sum-frequency generation (SFG) and difference-frequency generation (DFG). These nonlinear processes are illustrated in Fig. 2.4.

In SHG, two input photons with the same frequencies, f_1 are combined to generate $f_2 = 2f_1$. Similar to SHG, SFG combines two input photons at frequencies of f_1 and f_2 to generate f_3 (=$f_1 + f_2$). On the other hand, in DFG, the two input photons with frequencies f_3 and f_2 are combined to generate output wave at f_1 (=f_3- f_2). Note that in the case of DFG, in order for the energy to be conserved, there

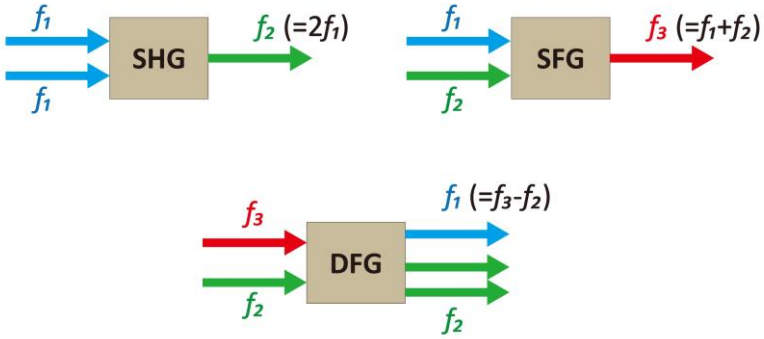

Fig.2.4 Illustrations of the common second-order nonlinear optical processes

must be two output photons at f_2 for each input photon at f_2. This process is also known as the optical parametric amplification.

All these second-order nonlinear effects will only be efficient when the combination of the photons is phase-matched, which refers to fixing the phase relation between the input photons throughout the nonlinear material. In materials, the refractive index is dependent on the frequency of the lights that propagates through it. Due to this, two photons with different frequency will have a variable phase relation as they propagate through the material, which causes the generated photons to be destructively interfering with each other. The solution to this phase-matching requirement is by employing quasi-phase matched (QPM) interactions in a periodically-poled nonlinear medium, where the sign of the nonlinear susceptibility is periodically reversed throughout the medium. By choosing the correct periodicity, which is to flip sign of the nonlinear susceptibility when the number of the generated photons at that point is at maximum as shown in Fig.2.5, the newly generated photons will always interfere constructively with the previous generated photons. As a result, the number of the generated photons will grow as the light propagates through the material, yielding high conversion efficiency.

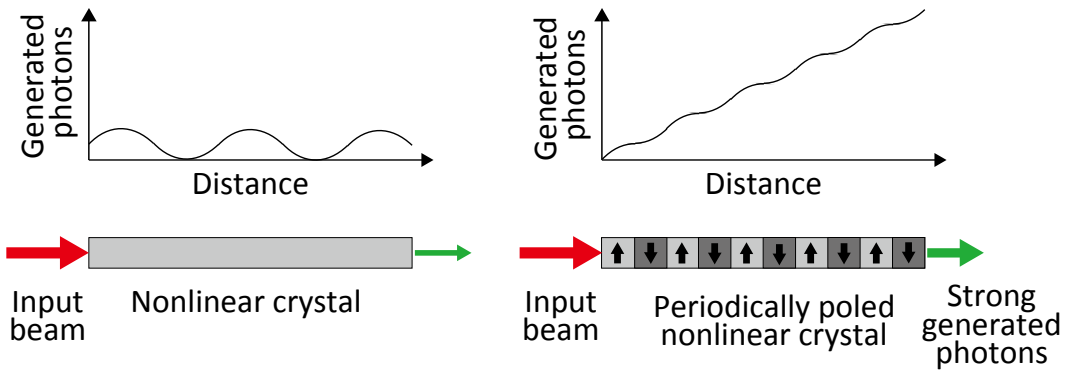

Fig. 2.5. The effect of quasi-phase matching on generated photons [Courtesy from *Comptes Rendus Physique* ***8****, 180 (2007)*]

2.3.3 Periodically-poled Lithium Niobate waveguide

Periodically-poled Lithium Niobate (PPLN) is a quasi-phase-matched material. In this research, PPLN waveguide is used as the medium for second-order nonlinear optical process in the optical frequency divider and the generation of high harmonics. Lithium niobate ($LiNbO_3$) is one of the most widely used nonlinear optical materials for frequency conversion applications because of its large nonlinear coefficient and broad spectral transmission. Waveguide media leads to efficiencies several orders of magnitude larger than those in bulk media, a result of the waveguide confinement eliminating the tradeoff between a small spot size and a long interaction length. Therefore, the application of PPLN waveguides as the nonlinear crystal results in a high conversion nonlinear process, thus, generates high power modes. Here, the definition of the conversion efficiency and the factors that influence the conversion efficiency are described.

Conversion efficiency

The generated output power P_{OUT} after propagating through a crystal with length of L is

$$P_{OUT} = \eta P_{IN1} P_{IN2} L^2 \tag{2-11}$$

with P_{IN1} and P_{IN2} being the two input power that are coupled into the crystal. η is the coupling efficiency of the beam into the crystal. The conversion efficiency is expressed as

$$\eta L^2 = \frac{P_{OUT}}{P_{IN1} P_{IN2}} \times 100 \ \ [\%/\mathrm{W}] \tag{2-12}$$

For SHG, this can be written as

$$\eta L^2 = \frac{P_{OUT}}{P_{IN1} P_{IN1}} \times 100 \ \ [\%/\mathrm{W}] \tag{2-13}$$

Conditions for optimum conversion efficiency

A) Coupling efficiency

In order to obtain high conversion efficiency, it is important to have a high coupling efficiency of the input lights into the PPLN waveguide. This can be achieved by designing the optical arrangement for best beam profile for the coupling process.

B) Polarization

In order to utilize the nonlinear properties of the lithium niobate, the polarization of the input beam must be aligned with the dipole moment of the crystal which is in the axis of the thickness of the crystal (e-polarization). If the beam is aligned orthogonal to the thickness of the crystal, the beam will be transmitted through the crystal without being converted. This applies to all nonlinear interactions.

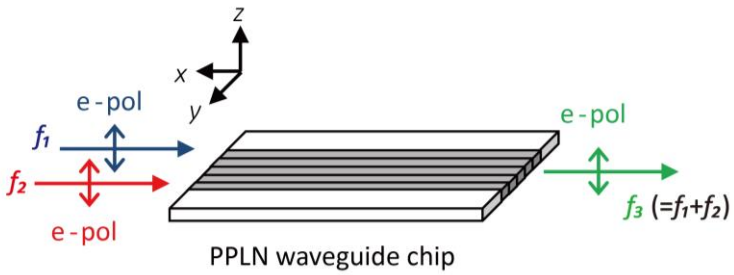

Fig.2.6: Polarization of input beams and generated beam in SFG process.

C) Temperature

The polling period of the crystal is determined by the target wavelengths to be used. This polling period can be changed by changing the temperature. Therefore, the QPM wavelengths can be slightly tuned by adjusting the temperature of the crystal. Highest conversion is obtained at the optimum temperature.

2.4 Pound-Drever-Hall technique

2.4.1 Introduction

The master laser used in the experimental design is a Littrow configuration external cavity diode laser (ECDL). One of the special features of the ECDL is that an adjustable diffraction grating inside the laser acts as a tuning element with a high selectivity. Furthermore, ECDL can offer lower phase noise and smaller emission linewidth (in single-frequency operation) compared to semiconductor lasers, distributed Bragg reflector (DBR) laser and distributed feedback (DFB) laser. However, frequency fluctuation still occurs around 100 MHz due to several possible reasons. For example, frequency fluctuation could be caused by the output fluctuation from the current controller and the temperature controller which depends on the accuracy and stability range of the equipment. In other words, even if the current controller is set at 80.0 mA, the actual current value could fluctuate within the range 79.95 mA ~ 80.04 mA. Furthermore, surrounding factors such as room temperature or movement on optical table could affect the inside gratings which influence the internal cavity length, thus resulting in fluctuation in oscillation frequency. In this study, it is important to control the frequency stability of the master laser in order to generate high harmonics with high precision. PDH technique is one of the common and very efficient methods for such purpose. In PDH technique, the frequency of the laser is stabilized by locking it to a highly stable reference cavity.

2.4.2 Principles of Pound-Drever-Hall technique

Generally, to stabilize a laser, one needs to prepare a reference with high precision and then lock the laser to the reference. In PDH technique, the frequency of the laser is stabilized by locking it to a highly stable reference cavity. This technique is performed by introducing the laser into the cavity and then uses the

reflected light from the cavity to produce a feedback to the laser. This feedback controls the oscillation frequency of the laser so that the intensity of the reflected light becomes constant at zero. However, it is important to note that the intensity of the reflected beam is symmetric to the resonance. If the laser frequency drifts out of resonance with the cavity, it is not possible to tell by just measuring the reflected intensity whether the frequency needs to be increased or decreased to bring it back onto resonance. The derivative of the reflected intensity (shown in Fig. 2.7), however, is antisymmetric to the resonance frequency. By giving a small variation to the frequency, an error signal can be obtained and used to lock the laser.

Above the resonance frequency, the derivative of the reflected intensity with respect to laser frequency is positive, as shown in Fig. 2.7. If a small range of variation is given to the laser frequency sinusoidally, the reflected intensity will vary sinusoidally as well, in phase with the variation in the frequency. Below the resonance frequency, this derivative is negative. On resonance the reflected intensity is at a minimum, and a small frequency variation will produce no change in the reflected intensity. By comparing the variation in the reflected intensity with the frequency variation, we can tell which side of resonance we are on. Once we have a measure of the derivative of the reflected intensity with respect to frequency, we can feed this measurement back to the laser to hold it on resonance.

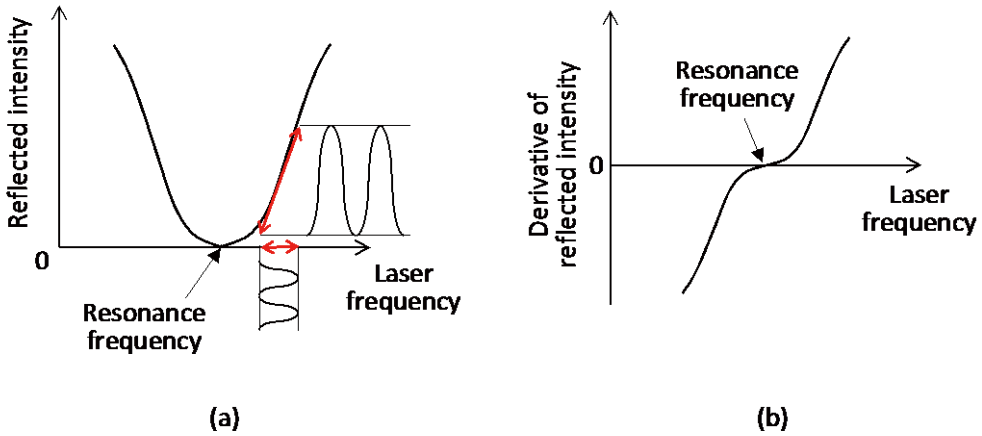

Fig. 2.7: (a) The reflected intensity from the reference cavity as a function of laser frequency, and (b) the derivative of the reflected intensity as a function of laser frequency, near resonance frequency.

2.4.3 Feedback process by Pound-Drever-Hall technique

Reflection coefficient of an optical cavity

The electric field of the incident beam on the Fabry-Perot cavity can be written as

$$E_{inc} = E_0 e^{i\omega t} \tag{2-14}$$

The reflected beam from the Fabry-Perot cavity is the coherent sum of two different beams; the promptly reflected beam, which bounces off the first mirror and never enters the cavity; and a leakage beam, which is the small part of the standing wave inside the cavity that leaks back through the first mirror. The leakage beam can be the sum of an infinite number of reflections inside the cavity. This sum of reflected beams can be written as

$$\begin{aligned} E_{ref} &= rE_{inc} + t^2 rE_{inc} e^{i\phi} + t^2 r^3 E_{inc} e^{i2\phi} + \cdots \\ &= \frac{r\left[e^{i\phi} - 1\right]}{1 - r^2 e^{i\phi}} E_{inc} \end{aligned} \tag{2-15}$$

where r is the reflection coefficient and t is the transmission coefficient of each mirrors of the cavity. Here, ϕ is

$$\phi = \frac{\omega}{\Delta\nu_{FSR}} \tag{2-16}$$

where $\Delta\nu_{FSR} = c/2L$ is the free spectral range of the cavity of length L. The transfer function F(ω) is the ratio of E_{ref} and E_{inc}, and for a symmetric cavity with no losses it is given by

$$F(\omega) = \frac{E_{ref}}{E_{inc}} = \frac{r\left[e^{i\phi} - 1\right]}{1 - r^2 e^{i\phi}} \tag{2-17}$$

If the cavity is resonating perfectly, or in other words, the laser's frequency is exactly an integer multiple of the cavity's free spectral range (FRS), then the

promptly reflected beam and the leakage beam have the same amplitude and are exactly 180° phase shifted. In this case, the two beams interfere destructively, and the reflection coefficient F(ω) becomes zero.

Generation of error signal

In Section 2.4.2, it is mentioned that a small variation needs to be given to the laser frequency for the PDH-locking process, but actually it is easier to modulate the phase rather than the frequency. The results are essentially the same but it is easier to describe the phase modulation mathematically.

After the beam is phase modulated by EOM, the electric field becomes

$$E(t) = E_0 e^{i(\omega t + \beta sin\omega_m t)} \tag{2-18}$$

Here, β is known as the modulation depth which indicates the performance of the modulator. This equation can be expended by using Bessel functions to

$$E(t) = E_0\left[J_0(\beta)e^{i\omega t} + J_1(\beta)e^{i(\omega+\omega_m)t} - J_1(\beta)e^{i(\omega-\omega_m)t}\right] \tag{2-19}$$

This equation shows that there are actually three different beams incident to the cavity; a carrier, with (angular) frequency ω, and two sidebands with frequencies $\omega \pm \omega_m$. Here, ω_m is the phase modulation frequency.

The reflected beam's field can be calculated by multiply each of the incident beams in Eq. (2-19) by the reflection coefficient. Therefore, the total reflected beam's field is

$$\begin{aligned} E_{ref}(t) = E_0\big[&F(\omega)J_0(\beta)e^{i\omega t} + F(\omega+\omega_m)J_1(\beta)e^{i(\omega+\omega_m)t} \\ &- F(\omega-\omega_m)J_1(\beta)e^{i(\omega-\omega_m)t}\big] \end{aligned} \tag{2-20}$$

However, the power of the reflected beam is the one that being measured by the photodetector. The power can be calculated by

$$
\begin{aligned}
P_{ref} &= \left|E_{ref}\right|^2 \\
&= P_c|F(\omega)|^2 + P_s[|F(\omega+\omega_m|^2 + |F(\omega-\omega_m|^2] \\
&+2\sqrt{P_cP_s}\{Re[F(\omega)F^*(\omega+\omega_m) - F^*(\omega)F(\omega-\omega_m)]cos\omega_m t \\
&+Im[F(\omega)F^*(\omega+\omega_m) - F^*(\omega)F(\omega-\omega_m)]sin\omega_m t\} \\
&+(terms\ in\ 2\omega_m\ )
\end{aligned}
\tag{2-21}
$$

Here, $P_c = {J_0}^2(\beta)P_0$ is the power in the carrier and $P_s = {J_1}^2(\beta)P_0$ is the power in each first-order sideband.

When the carrier is near resonant and the modulation frequency is high enough that the sidebands are not, we can assume that the sidebands are totally reflected, $F(\omega \pm \omega_m) \approx -1$. Then the quantity

$$F(\omega)F^*(\omega+\omega_m) - F^*(\omega)F(\omega-\omega_m) \approx -i2Im\{F(\omega)\}.$$

is purely imaginary. In this regime, the cosine term in Eq. (2-21) is negligible, and the power component that becomes the error signal ε can be written as

$$\varepsilon = -2\sqrt{P_cP_s}Im[F(\omega)F^*(\omega+\omega_m) - F^*(\omega)F(\omega-\omega_m)]sin\omega_m t \tag{2-22}$$

In order to generate the actual error signal from Eq. (2-22), the optical signal needs to be converted to electric signal, and then mixed with a reference signal. Finally, only the DC component of the signal is filtered through a low pass filter. The details of the process are as follows. First, the optical signal is converted to an electric signal, $V_\varepsilon sin\omega_m t$, where V_ε is the amplitude ($V_\varepsilon \propto -2\sqrt{P_cP_s}Im[F(\omega)F^*(\omega+\omega_m) - F^*(\omega)F(\omega-\omega_m)]sin\omega_m t$). This signal is then mixed with a phase-shifted reference signal from a local oscillator $V_0\sin(\omega_m t+\phi)$ (ϕ : phase difference between signal detected by photodetector and reference signal) in a double balanced mixer (DBM), generating the following signal,

$$V_\varepsilon sin\omega_m t \cdot V_0\sin(\omega_m t+\phi) = \frac{V_\varepsilon V_0}{2}cos\phi - \frac{V_\varepsilon V_0}{2}\cos(2\omega+\phi) \tag{2-23}$$

where ϕ is constant. The signal from Eq. (2-23) is filtered so that only the DC component is picked out. The filtered DC signal can be written by

$$S(\omega) = \frac{V_\varepsilon V_0}{2} cos\phi \tag{2-24}$$

This $S(\omega)$ is the error signal used in the PDH method, which is to feed back to the ECDL.

Near the resonance, the error signal can be viewed as a straight line with a certain inclination. This inclination is an important element to the error signal. The reason is that, for a highly accurate locking, the error signal should be changing drastically at near resonance, where the resonance becomes like a mirror that reverses the positive and negative error signal with a steep inclination. The steeper the inclination means higher accuracy of the PDH locking, thus resulting in further stabilization of the laser's frequency. The error signal near resonance can be written as

$$\varepsilon = -\frac{8\sqrt{P_c P_s}}{\delta\nu}\delta f \equiv D\delta f \tag{2-25}$$

Where, $\delta\nu$ is the cavity's linewidth and δf is the deviation of laser's frequency from the resonance frequency.

From Eq. (2-25), it is understood that when the lasers' power P_c and P_s is constant, the inclination D can be increased by decreasing the cavity's linewidth $\delta\nu$. In other words, a high inclination D can be obtained by using an optical cavity with high Finesse or optical cavity with small FSR.

Examples of error signal

Figure 2.8 shows some examples of error signal as frequency sweep is given to the laser's frequency, where the relative phase difference, between the detected signal and the reference signal ϕ is varied. Here, the reflectance is 99.84% (finesse=2000), FSR = 2.0 GHz and frequency modulation = 19.4 MHz. At ϕ = 0 and π rad, the peak-to-peak value of the error signal is at maximum. At $\phi = \pi/2$ rad, the peak-to-peak value of the error signal is at minimum. Furthermore, $\phi = \pi/2$ rad is the changing point where the positive and negative signal is reversed. The feedback signal to ECDL needs to satisfy the followings:

- Signal that gives positive voltage feedback when the laser's frequency shifts to lower frequency and negative voltage feedback when the laser' frequency shifts to higher frequency, so that the frequency shift always stay at zero.
- Signal with maximum peak-to-peak value of the inclination part, and wide locking range (with resonance frequency as the center frequency).

As a conclusion, the error signal in Fig. 2.8 (a) , in which the ϕ = 0 rad, satisfies all the requirements above, and this signal is used in the feedback process to master laser in the experimental system.

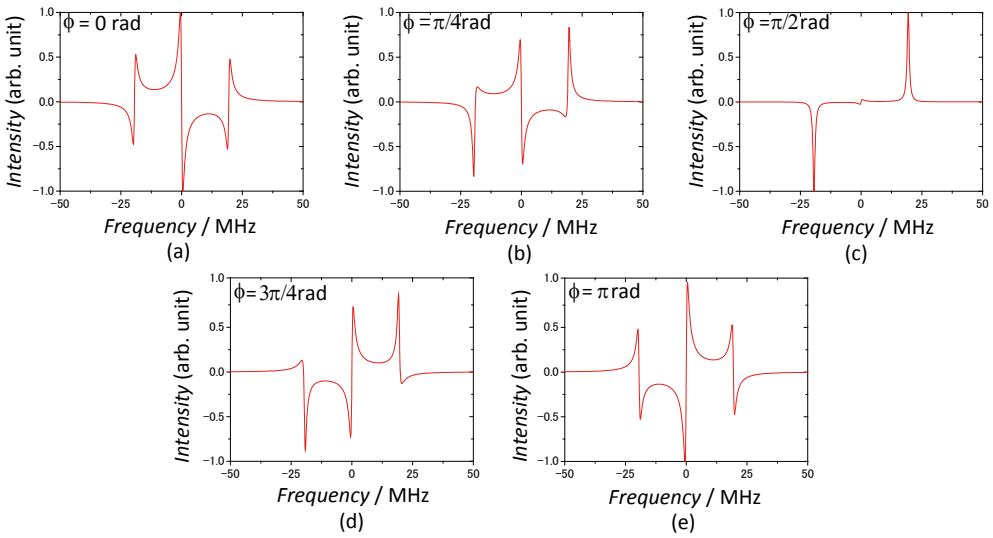

Fig.2.8: Examples of error signal during frequency sweep at different phase difference, ϕ. (a) ϕ = 0 rad, (b) ϕ = π/4 rad, (c) ϕ = π/2 rad, (d) ϕ =3π/4 rad, (e) ϕ = π rad.

2.5 Harmonics interference

2.5.1 Introduction

After a total of five harmonics has been generated, it is necessary to clarify the phase coherence among them in order to determine their potential for specific applications, for example the AOW generation, where a constant phase relationship is necessary. Since the generated five frequencies are multiple harmonics of the fundamental frequency, second harmonic of any components or the sum of any two components that result in the same value of frequency can be heterodyned to demonstrate the phase coherence among the harmonics.

Here, a theoretical study is shown to estimate the interference fringe between the generated harmonics.

2.5.2 Concept of harmonics interference

Figure 2.9 shows the conceptual illustration of optical phase manipulating method for observing the phase interference between the harmonics. The phase of the harmonics is manipulated by changing their optical path length by inserting a pair of glass plates in the optical path and tilting them symmetrically.

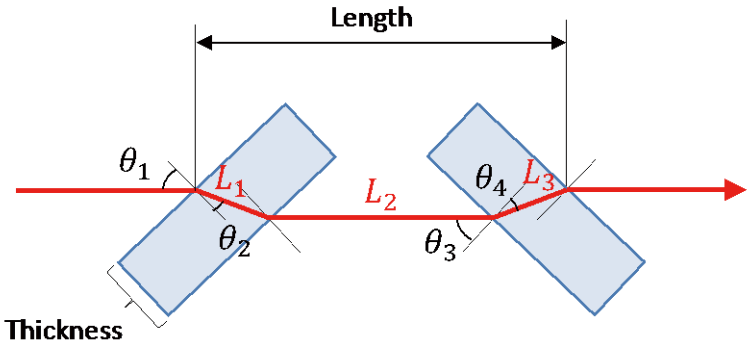

Fig. 2.9: Conceptual illustration of phase manipulating method by employing glass plate pair

The optical path length from the input surface of the first plate to the output surface of second plate is different for each wavelength λ. This is because the diffraction index of the glass material depends on the wavelength.

First, the diffraction angle of each wavelength is defined as follows,

$$\theta_1: \text{input angle} \tag{2-26}$$

$$\theta_2(\lambda) = \text{Sin}^{-1}\left[\frac{n_{air}}{n_{glass}(\lambda)}\text{Sin}\theta_1\right] \tag{2-27}$$

$$\theta_3 = \theta_1 \tag{2-28}$$

$$\theta_4(\lambda) = \text{Sin}^{-1}\left[\frac{n_{air}}{n_{glass}(\lambda)}\text{Sin}\theta_3\right] \tag{2-29}$$

Where n_{air} is the refractive index of air, n_{glass} is the refractive index of the glass material which is determined by Sellmeier's equation.

The path length is defined as

$$L_{path} = L_1 + L_2 + L_3 \tag{2-30}$$

Where

$$L_1 = \frac{Thickness}{Cos\ \theta_2(\lambda)} \tag{2-31}$$

$$L_2 = Length - \frac{Thickness}{Cos\theta_2(\lambda)} Cos[\theta_1 - \theta_2(\lambda)] - \frac{Thickness}{Cos\theta_4(\lambda)} Cos[\theta_3 - \theta_4(\lambda)] \tag{2-32}$$

$$L_3 = \frac{Thickness}{Cos\ \theta_4(\lambda)} \tag{2-33}$$

The phase of each wavelength will be

$$\phi(\lambda) = 2\pi \left[\frac{L_1 + L_3}{\lambda / n_{glass}(\lambda)} + \frac{L_2}{\lambda / n_{air}} \right] \tag{2-34}$$

In the case of heterodyning SFG of f_2 and f_5 and SFG of f_3 and f_4 ,the interference term can be defined by the following term.

$$|exp[\mathbb{i}\phi_{SFG1}] + exp[\mathbb{i}\phi_{SFG2}]|^2 \tag{2-35}$$

Here, $\phi_{SFG1} = \phi_2 + \phi_5$ and $\phi_{SFG2} = \phi_3 + \phi_4$.

By plotting the interference term using the same condition as used in the actual experimental setup, the actual interference fringe can be estimated.

References for Chapter 2:

1. R. Wynands, T. Mukai, and T. W. Hansch, “Coherent bisection of optical frequency intervals as large as 530 THz”, Opt. Lett. 17, 1749 (1992).
2. J. E. Bernard, B. G. Whitford, and L. Marmet, “Phase-locked optical divide-by-3 system for visible radiation”, Opt. Lett. 24, 98 (1999).
3. N. Chiodo, F. Du-Burck, J. Hrabina, M. Lours, E. Chea, and O. Acef, “Optical phase locking of two infrared continuous wave lasers separated by 100 THz”, Opt. Lett. 39, 2936 (2014)

Chapter 3

Experimental setup

3.1 Introduction

In this chapter, I will explain the experimental setup to generate five phase-locked harmonics by implementing a divide-by-three optical frequency divider. The schematic of the whole experimental setup and the picture of the actual setup are shown in Fig. 3.1 and Fig 3.2, respectively. The system is divided into three main elements, a master laser that is stabilized by a Pound-Drever-Hall (PDH) technique (detailed in section 3.3), a divide-by-three optical frequency divider (detailed in section 3.4) and a high harmonics generation system that applies second-order nonlinear optical processes (detailed in section 3.5). The experimental scheme can be briefly explained as follows; first, the master laser is stabilized to a reference cavity by PDH technique. Then, the radiation of the master laser is applied together with a divider laser radiation into the divide-by-three optical frequency divider to generate three phase-locked harmonics with a frequency ratio of exact 1:2:3. At the high harmonics generation system, these three phase-locked harmonics are introduced into two PPLN waveguides sequentially to generate another two higher harmonics by SFG processes. The measurement of the spectral

phase stability among the generated five harmonics is detailed in section 3.6.

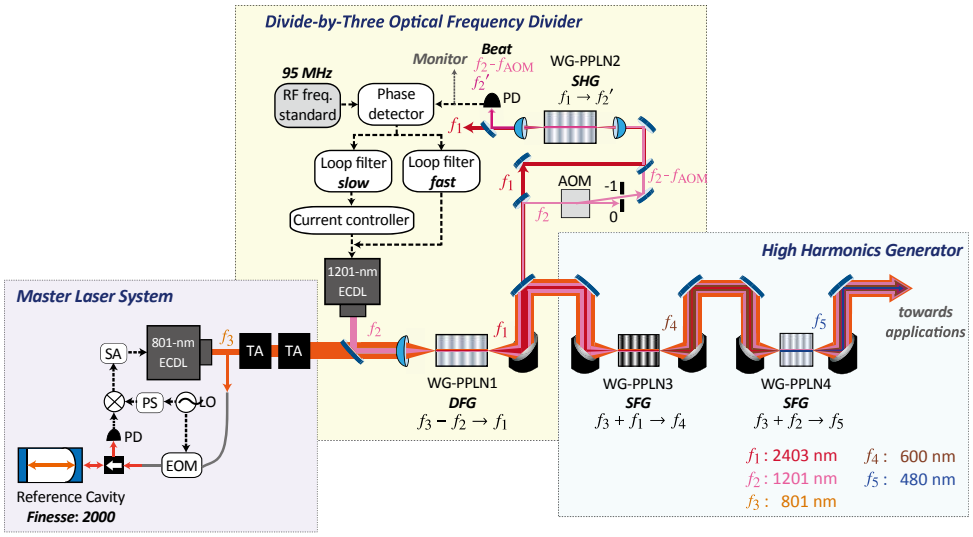

Fig. 3.1: Schematic of experimental setup for generating five phase-locked harmonics. This system is divided into three main parts; master laser, divide-by-three optical frequency division and high harmonics generation. ECDL: external cavity diode laser, TA: tapered amplifier, EOM: electro-optic modulator, LO: local oscillator, PS: phase shifter, SA: servo amplifier, PD: photo detector, WG-PPLN: periodically poled lithium niobate waveguide, AOM: acousto-optic modulator, DFG: difference frequency generation, SFG: sum frequency generation, SHG: second harmonic generation.

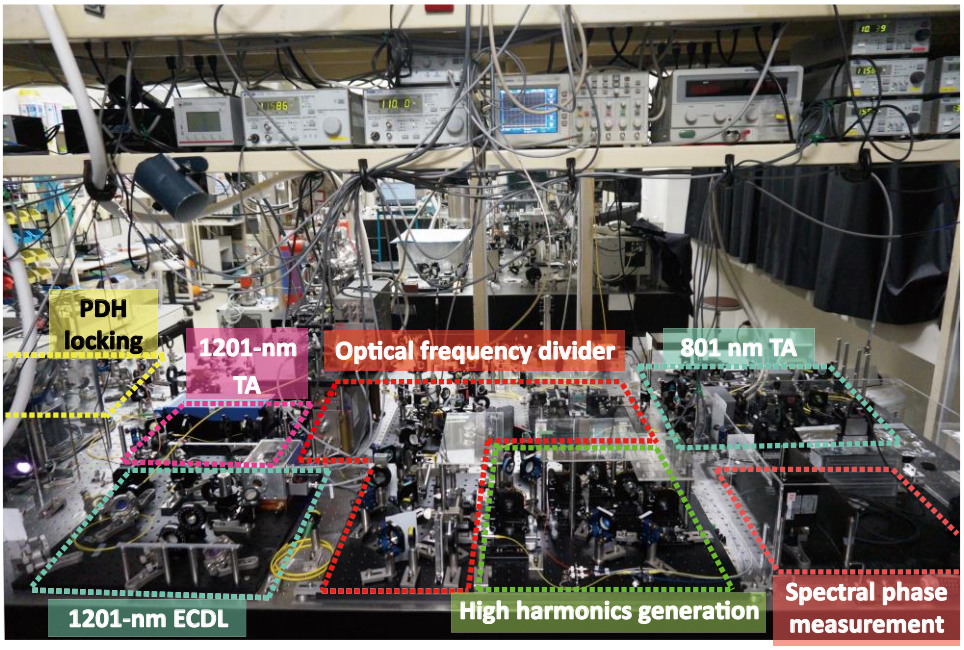

Fig. 3.2: Picture of actual experimental setup for generating five phase-locked harmonics.

3.2 Periodically-poled Lithium Niobate (PPLN) waveguide as nonlinear optical medium

In the experimental design, periodically poled lithium niobate (PPLN) waveguide is used as the nonlinear medium for DFG and SHG processes in the optical frequency divider system and for SFG processes in the high harmonics generation system. In this section, the structure of the PPLN waveguide chip and the operating condition for optimum conversion efficiency will be described.

Structure of PPLN waveguide chips

Figure 3.3 shows the schematic of a PPLN waveguide chip (from NTT-Advanced Technology) used in this study. The chip consists of twelve waveguides which are

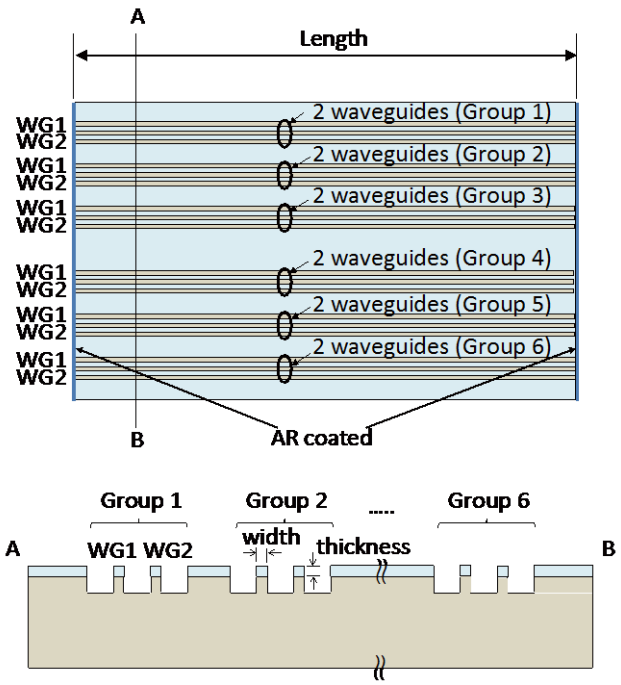

Fig. 3.3: Structure of a PPLN waveguide chip [Courtesy from *NTT Electronics*]

divided in pair into six groups. Each waveguide has different width and quasi-phase matching (QPM) pitch for different condition of phase-matching process. The length of the PPLN waveguide chip is designed based on the targeted nonlinear process.

In the experimental design, a total of four PPLN waveguide chips are used for three different types of frequency mixing process; DFG, SHG and SFG. Table 1 shows the dimensions of the waveguide chip for each process.

Table 1 Dimensions of PPLN waveguide for different type of nonlinear mixing processes.

Chip no. (Group, waveguide)	Nonlinear process (wavelength)	QPM pitch (μm)	Width (μm)	Thickness (μm)	Length (mm)
WG-PPLN1 (Group 1 WG 1)	DFG (1201 nm, 801 nm → 2403 nm)	20.22	12.3	10	48
WG-PPLN2 (Group 2 WG 2)	SHG (2403 nm → 1201 nm)	31.34	11.9	10	48
WG-PPLN3 (Group 2 WG 2)	SFG (2403 nm, 801 nm → 600 nm)	11.65	11.7	10	34
WG-PPLN4 (Group 1 WG 2)	SFG (1201 nm, 801 nm → 480 nm)	11.63	7.8	7.3	23

* The full data on the PPLN waveguide chips is shown in Appendix A1

Operating conditions

As described in Section 2.3, the conversion efficiency in a PPLN waveguide depends on the coupling efficiency of the input beams and the phase-matching conditions for the target wavelengths. The coupling efficiency is controlled by the optical arrangement whereas the phase-matching condition is controlled by the temperature of the PPLN and the polarization of the input beams. Here, the optimum conditions for each PPLN are clarified.

A) Optical arrangement and coupling efficiency

The optimum coupling efficiency is obtained when the input beam profile matches the single-transverse mode condition inside the waveguide. In the actual experimental setup, this condition is obtained by adjusting the input beam profile while observing the profile of the output beam and the coupled power. An aspheric lens with focal length of 4.51 mm is used to couple 801-nm beam into WG-PPLN1. The maximum coupling efficiency obtained is 92%, which is considered as high. However, in the case of coupling a multiple-wavelengths beam with broad bandwidth, it is impossible to get the same high coupling efficiency in a good single-transverse mode for all wavelengths by using a focusing lens due to the aberration effect. Therefore, in the actual experimental system, parabolic mirrors with focal length of 15 mm are used for WG-PPLN3 and WG-PPLN4, which are to couple more than three wavelengths. Table 2 shows the optimum coupling efficiency for each PPLN waveguides used in this study.

Table 2 Coupling efficiency at each PPLN waveguide

	Focusing optics	Input wavelength (nm)	Coupling efficiency (%)
WG-PPLN1	Aspheric lens, f = 4.51 mm	801 1201	92 84
WG-PPLN2	Aspheric lens, f = 4.00 mm	1201 2403	18 43.5
WG-PPLN3	Parabolic mirror, f = 15 mm	801 1201 2403	81 80 66
WG-PPLN4	Parabolic mirror, f = 15 mm	600 801 1201 2403	46 57 54 24.5

B) Temperature

The optimum temperature for each PPLN waveguides is verified by monitoring the output power of the generated wavelength. In this study, the optimum temperature for WG-PPLN1, WG-PPLN2, WG-PPLN3 and WG-PPLN4 for the target wavelengths is 98, 95, 51.2 and 50.65 °C, respectively. However, in the actual operation, the operating temperature of WG-PPLN3 is set to 52.3 °C because at the optimum temperature, the output power of 1201 nm decreases in a huge amount due to the conversion process. Therefore the operating temperature is shifted a little bit from the optimum temperature to balance the final output powers for all wavelengths for the next applications.

C) Conversion efficiency

At the coupling efficiency and operating temperature as mentioned above, the conversion efficiency at each PPLN waveguides is measured and defined by using Eq. (2-7) and (2-8). The results are shown in Table 3.

Table 3 Conversion efficiency of each PPLN waveguides

	Nonlinear process (wavelength)	Conversion efficiency (%/W)
WG-PPLN1	DFG (1201 nm, 801 nm → 2403 nm)	420.5
WG-PPLN2	SHG (2403 nm → 1201 nm)	121.6
WG-PPLN3	SFG (2403 nm, 801 nm → 600 nm)	149
WG-PPLN4	SFG (1201 nm, 801 nm → 480 nm)	235.2

3.3 Master laser stabilization by using Pound-Drever-Hall technique

Figure 3.4 shows the PDH system used in the experimental design to stabilize the master laser. First, the radiation from the ECDL is coupled into a single-mode optical fiber. The radiation power is divided into two parts by using a 90:10 fiber divider; 90% is sent towards tapered amplifier for further application, and 10% is used for PDH locking. For the PDH locking, the frequency of radiation is modulated by a fiber-coupled electro-optical modulator (EOM) driven by a local oscillator with frequency modulation of 20 MHz. It is not shown in Fig 3.4 but there is a half-wave plate and a polarization beam splitter at the EOM input to match the polarization of the laser to the EOM polarization characteristic. The frequency-modulated light is then introduced into a reference cavity with finesse of 2000. The reflected radiation is picked off with an optical isolator and sent into a photo-detector to transform the intensity information into an electrical signal. This electric signal is then compared with the local oscillator's signal via a mixer. A low pass filter on the output of the mixer isolates the low frequency signal, which contains the information of the derivative of the reflected intensity. This low frequency signal will go through a servo circuit and into the tuning port on the laser, locking the laser to the cavity.

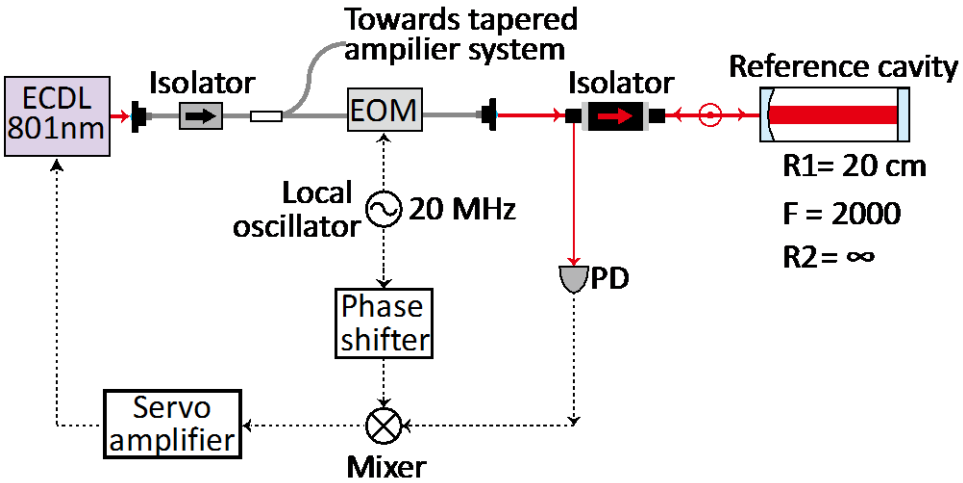

Fig. 3.4: Layout of the actual PDH system in this study. ECDL: external-cavity diode laser, EOM: electro-optic modulator, PD: photodetector.

3.4 Divide-by-three optical frequency divider

Figure 3.5 shows the experimental system layout of the divide-by-three optical frequency division method to generate the initial three phase-locked harmonics, f_1, f_2 and f_3. ECDLs that oscillate at 801 and 1201 nm are used as the master (f_3) and divider (f_2) lasers, respectively. The oscillation frequency of the master laser is stabilized to a reference cavity with the Pound-Drever-Hall (PDH) method as explained in Section 3.3. The output power from the master laser system is ~10 mW and is followed by two tapered amplifiers (TA) that increase the power to 1 W, approximately (TA system is described in the Appendix). The output power of the divider 1201-nm ECDL is 12 mW. The 801- and 1201-nm radiations are coupled in space with a dichroic mirror and introduced into a periodically poled lithium niobate waveguide, WG-PPLN1 to generate the difference frequency, $f_3 - f_2 = f_1$: 2403 nm. This DFG process, which also acts as an optical parametric amplifier (OPA), increases the power of f_2: 1201-nm radiation simultaneously. As a result, at the exit of WG-PPLN1, we obtained output powers of 810, 80, and 39 mW for 801-, 1201-, and 2403-nm radiations, respectively. From these output powers, 2 mW of 1201-nm radiation and 20 mW of 2403-nm radiation are segregated for the phase locking line. The remaining power is used for the main beam line for generating the phase-locked high harmonics through nonlinear optical mixing processes.

At the phase-locking beam line, first, the 2403- and 1201-nm radiations are separated into an individual line. Then, a frequency shift of -95 MHz is given to the 1201-nm radiation using an acoustic optical modulator (AOM). The 2403-nm and the frequency-shifted 1201-nm radiations are recombined in space and introduced into WG-PPLN2 to generate the second harmonic of the f_1: 2403-nm radiation. At the exit of WG-PPLN2, output powers of 14 and 180 μW were obtained for second harmonic of f_1: 2403-nm radiation and frequency-shifted 1201-nm radiation, respectively. The generated second harmonic, f_2' and the frequency-shifted 1201-nm (f_2 – 95 MHz) radiations are heterodyned in a high-speed photo-diode and their RF beat signal (95 MHz + f_2' – f_2) is detected. This RF beat signal is further mixed with a 95-MHz RF standard using a phase detector for generating an error signal. The phase detector employed here has a broad response bandwidth of 200 MHz, which consists of an ultrafast dual comparator (Analog Device AD96687) and a phase and frequency discriminator (Analog Device AD9901). Finally, the obtained error signal

is fed back to the current of the divider laser, the 1201-nm ECDL; one is through the current controller with a slow feedback of < 100 kHz, the other to the ECDL directly with a fast feedback of < 1.5 MHz (The details of the current feedback are explained in the next part of this section). In this way, the divide-by-three optical-frequency division can be achieved, which results in the generation of three phase-locked harmonics, f_1: 2403 nm, f_2: 1201 nm and f_3: 801 nm.

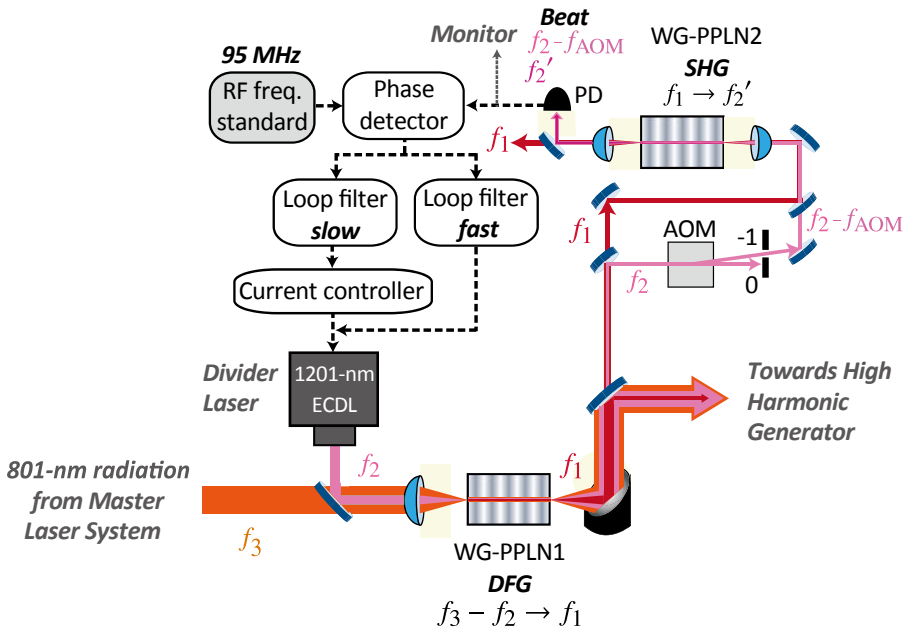

Fig. 3.5: System layout of the divide-by-three optical frequency division. ECDL: external cavity diode laser, TA: tapered amplifier, PD: photo detector, WG-PPLN: periodically poled lithium niobate waveguide, AOM: acousto-optic modulator, DFG: difference frequency generation, SHG: second harmonic generation.

Design of current feedback system

First, a digital phase detector is built to compare the phase difference between the beat signal and the reference signal for producing the error signal. Then, the ECDL response towards current modulation is analyzed to clarify the frequency limit of current modulation that can be fed to the ECDL without causing phase delay. Also, the delay time of the error signal to go through one complete loop is estimated based on the length of electronic cable and optical path in the loop. Based on these data, the loop filter is designed to compensate the phase delay. Finally, these data are used to estimate the characteristic of the current feedback system.

A) Digital phase detector

A digital phase/frequency discriminator (Analog Device AD9901) is used as a phase detector in this work. Its major feature is its capability to directly compare phase/frequency inputs up to 200 MHz. This IC operates in two distinct modes; as a linear phase detector and as a frequency discriminator. When the two input signals (beat signal and oscillator signal) are very close in frequency, only the phase detection mode is on. If the two inputs are substantially different in frequency, the frequency discrimination mode overrides the phase detection mode to pull back in the two input frequencies within the range of phase detector. Even if a fault occurs that causes the frequencies to be out of the phase detector range, the frequency discriminator will pull them back in. In other words, the advantage of this IC is that the detection range is wide and the phase-locking condition can be really stable. Furthermore, the linear phase detection makes the error signal becomes easy to be analyzed.

The only disadvantage is that the signals need to be converted to digital signals by a dual high-speed comparator (Analog Device AD96687), which adds a little bit of propagation delay due to the characteristic of the comparator.

At the output of AD9901, an offset control circuit is added to increase the gain as shown in Fig. 3.6. The G_ϕ of the AD9901 is 0.2865 [V/rad]. After the gain is increased to five times, G_ϕ = 1.4325 [V/ rad].

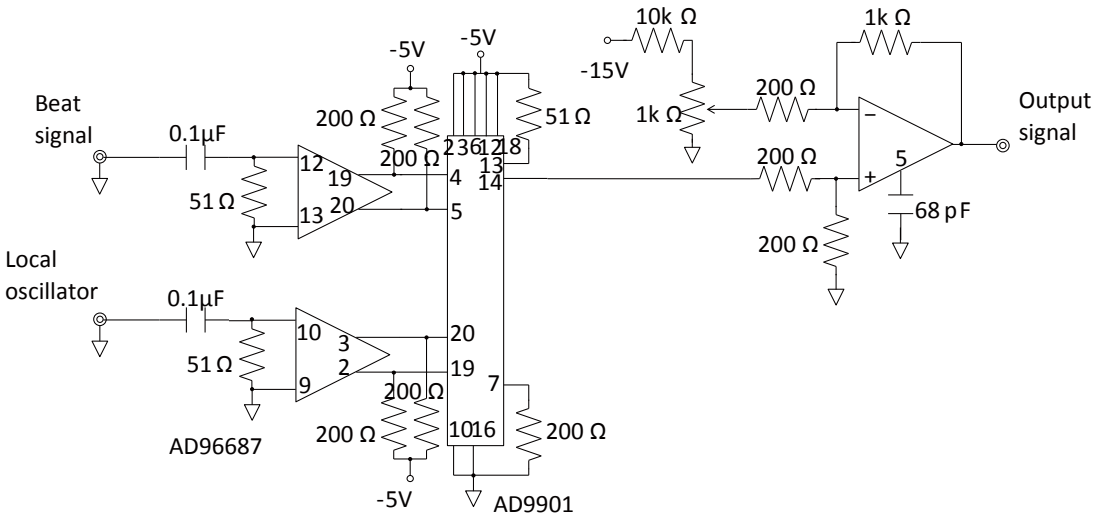

Fig. 3.6 Design of digital phase detector and offset control circuit

B) ECDL response

The current feedback in this work is applied to the ECDL. Hence, it is important to understand the characteristics of the laser diode in order to design the servo circuits for the feedback process. Temperature change in the laser diode gives influence to the oscillating frequency. This is because, when the temperature increases, the cavity length will expands, which causes the increase of wavelength, thus results in lower frequency. On the other hand, if the temperature decreases, the frequency will get higher. Therefore, by controlling the current into the laser diode, not only will change the power but also will change the oscillating frequency due to the heat generated by the current. For this reason, it is important to know the characteristics of the ECDL towards the current change. For this purpose, frequency modulation is given to the current controller. Figure 3.7 shows the measured gain and phase shift characteristics of the ECDL when frequency modulation is given to the current controller.

The limit of phase delay is 45 degree. From the phase shift characteristic, phase delay is marked at 56 degree because of offset value of 11 degree. At this point, the frequency value is 340 kHz. This indicates that the frequency tuning limit for the ECDL, α = 340 kHz. At this point, we can also see that the gain decreases. The phase delay and gain decreases are compensated by a phase advance filter in the loop filter. The rate of oscillating frequency shift to the current change, G_d is 8.64×10^{11}.

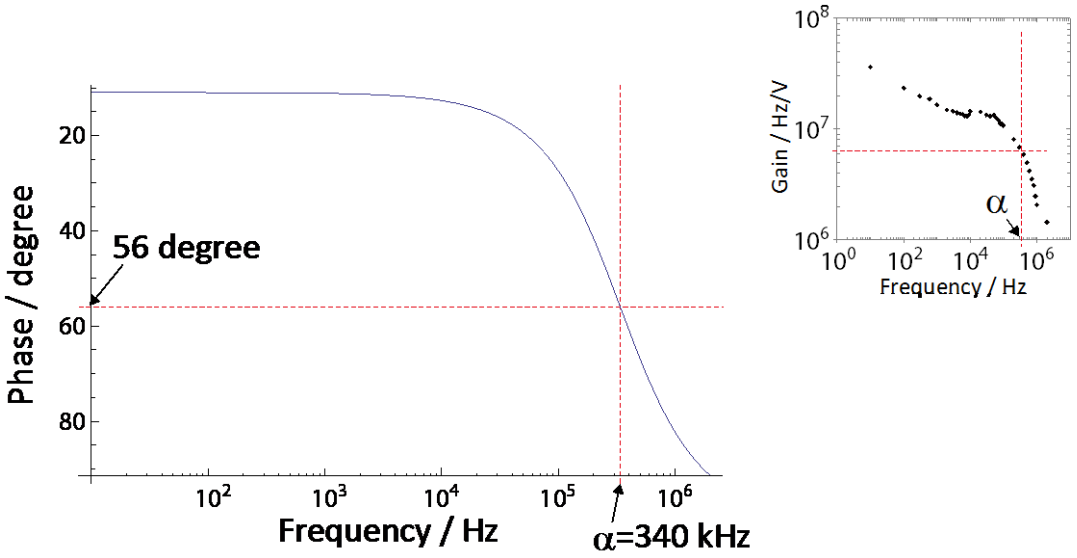

Fig. 3.7: Characteristics of 1201 nm ECDL towards frequency modulation on the current controller

C) Loop filter design

In the system, I used two loop filters for the feedback process. For the slow feedback, I used a commercial servo circuit (D2-115, Vescent Photonics). For the fast feedback I used a handmade circuit. The commercial servo circuit can only respond to the error signal below 1 MHz without phase delay. The fast loop circuit is designed to compensate the decrease of gain and the phase delay that occurs at the frequency α as mentioned above. The fast loop circuit is shown in Fig. 3.8. The characteristic of this loop circuit (measured by using a network analyzer) is shown in Fig. 3.9.

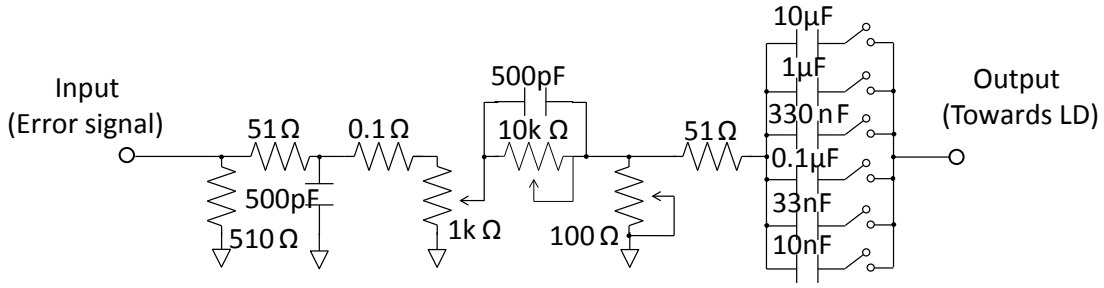

Fig. 3.8: Design of loop filter circuit for fast feedback.

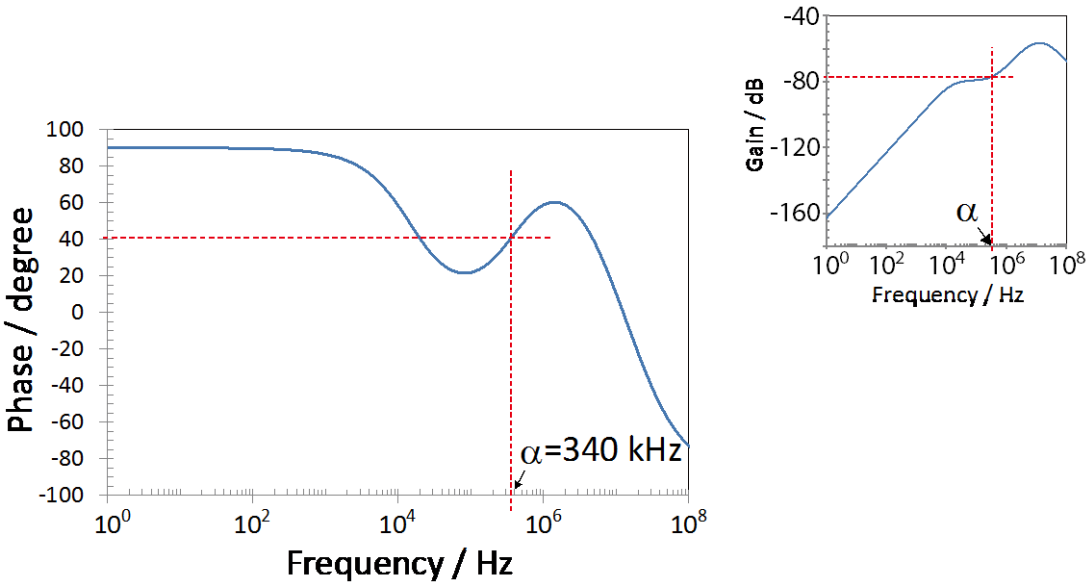

Fig. 3.9: Characteristics of fast loop filter circuit for fast feedback.

Figure 3.9 shows that the loop filter compensates the phase delay and gain decrease at α = 340 kHz.

D) Delay

The delay time τ is estimated from the length of light propagations and the electronic cable length, which is 35×10^{-9} sec.

From the transfer functions of each element, the characteristics of the current feedback system are estimated by using open-loop function from (2-10) in Section 2.2 and the result is shown in Fig. 3.10.

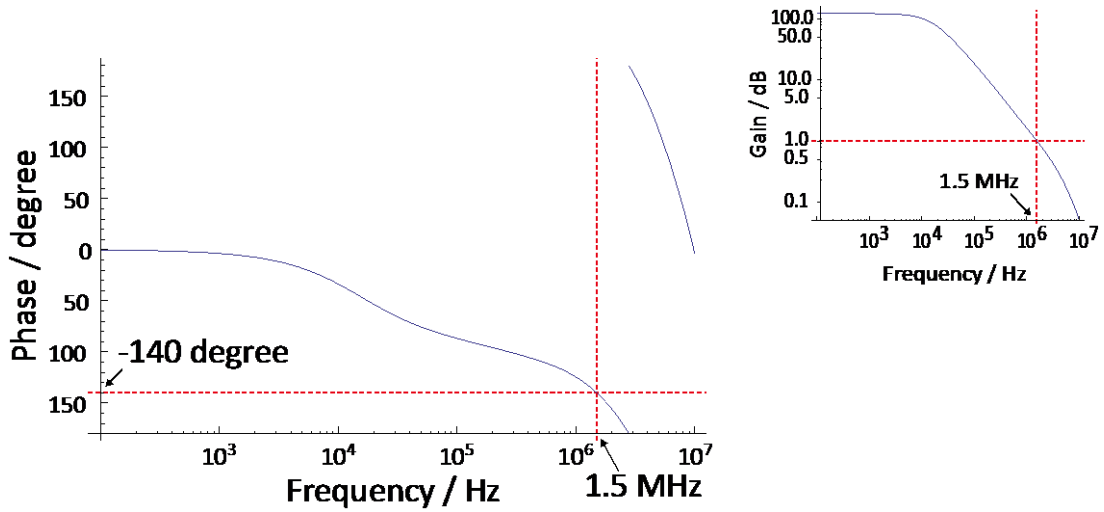

Fig. 3.10: Characteristics of current feedback system.

From Fig. 3.10, it is understood that at phase delay of -140 degree (40 degree margin is given before π) the frequency is at 1.5 MHz. This value indicates that the estimated phase noise that can be compensated by the current feedback system is limited to 1.5 MHz. Based on the bandwidth of the beat spectrum at the free running condition (shown in Fig. 5.2), 1.5 MHz is sufficient. Furthermore, the gain is set to 1 dB at 1.5MHz so that the gain of the loop filter can be adjusted within the feedback limit.

The overall circuit design for current feedback is shown in Fig. 3.11.

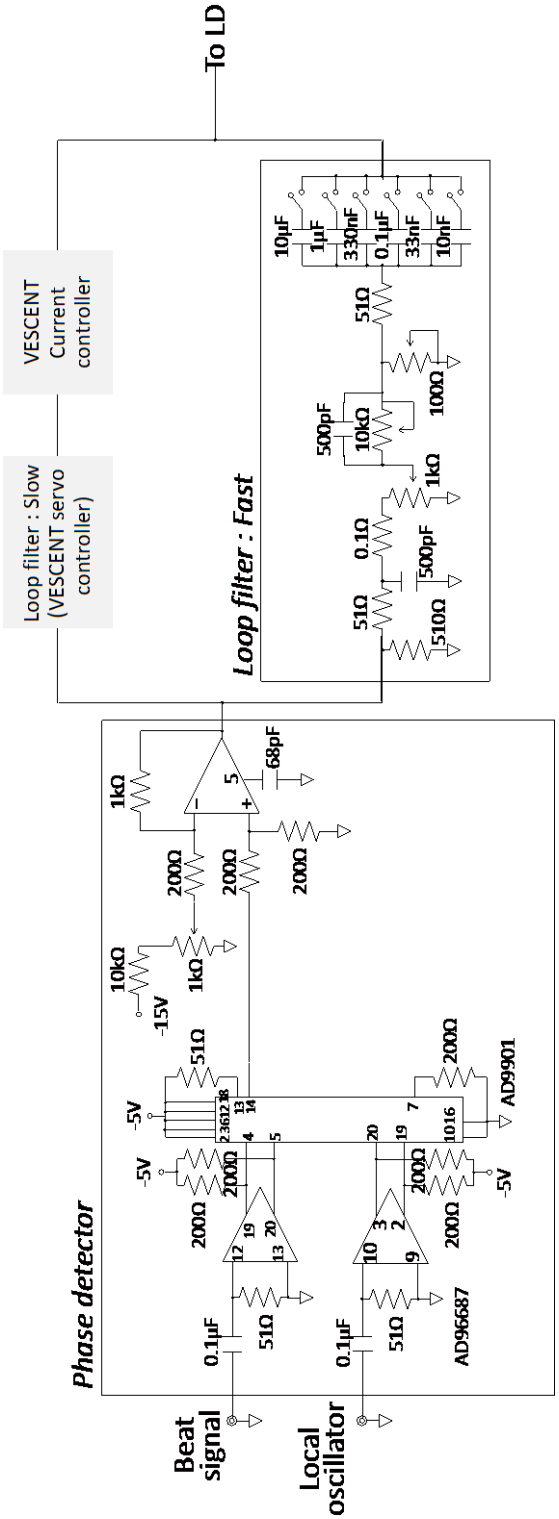

Fig. 3.11: Schematic of overall circuit design for current feedback

3.5 High harmonic generation

The experimental setup for high harmonics generation is shown in Fig. 3.12. The three phase-locked harmonics from the divide-by-three optical frequency divider are introduced into two periodically poled lithium niobate waveguides, WG-PPLN3 and WG-PPLN4 sequentially to generate the f_4: 600-nm and f_5: 480-nm harmonics by mixing f_1: 2403-nm and f_3: 801-nm radiations and f_2: 1201-nm and f_3: 801-nm radiations, respectively. At the WG-PPLN3 input, the power of f_1, f_2 and f_3 is 810, 78 and 18.6 mW, respectively. After conversion, power obtained at WG-PPN3 output is 3.3, 62.4, 653 and 12 mW for f_1, f_2, f_3 and f_4, respectively. These four radiations are directly introduced into WG-PPLN4 to generate the fifth harmonic, f_5. Note that all the harmonics are coupled coaxially from one waveguide to another by using parabolic mirrors (focal length: 15 mm, Ag coated) in order to avoid chromatic aberration. This coaxial layout of the entire system is practically significant in terms of application, since the phase-locked nature among all the harmonics can be robustly maintained against disturbances.

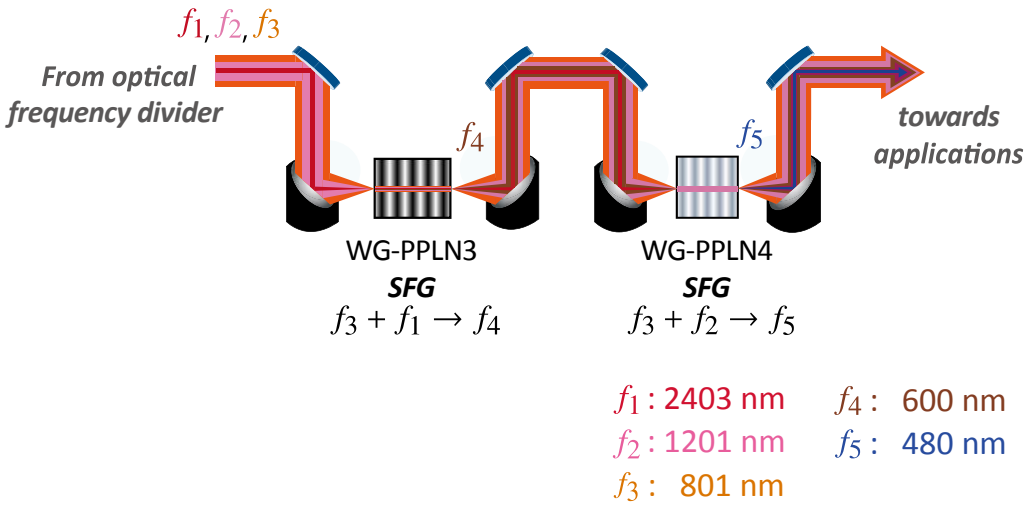

Fig. 3.12: Experimental layout of the high harmonics generation system. WG-PPLN: periodically poled lithium niobate waveguide, SFG: sum-frequency generation.

3.6 Spectral phase measurement

Since the generated five frequencies with wavelengths of 2403, 1201, 801, 600 and 480 nm are multiple harmonics of the fundamental frequency, there are four pairs of SHG and SFG that result in the same frequency: (a) SFG of 2403 and 801 to SHG of 1201 nm, (b) SFG of 2403 and 600 to SFG of 1201 and 801 nm, (c) SFG of 1201 and 480 to SFG of 801 and 600 nm, and (d) SFG of 801 and 480 to SHG of 600 nm. For this dissertation, the combination in (c) is chosen for interference measurement because of the spectral power factor.

Figure 3.13 shows the schematic picture of the experimental setup for interference measurement. The relative spectral phases of the five harmonics are altered by changing their optical path length via inserting a pair of Calcium Fluoride plates (thickness: 5 mm) in the optical path after WG-PPLN4 and tilting them symmetrically with exactly the same angle of α (this phase manipulation is described in detail in Refs. 1, 2). The BBO crystal is cut for type-I phase-matched SHG and SFG of the five frequencies. The sum frequency component (named f_7^{β}) was generated in two ways in the BBO crystal (Type I phase-matching, thickness: 10 μm), namely SFGs via f_2:1201 nm + f_5:480 nm and f_3:801 nm + f_4:600 nm. A band-pass filter was used to only allow the f_7^{β} components to be superimposed onto a photo detector.

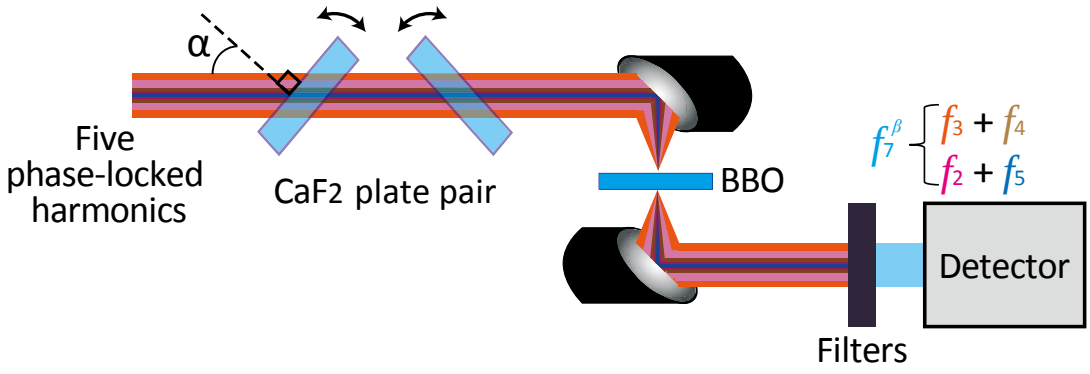

Fig. 3.13: Experimental layout for measuring interference signal aroused with two superimposed f_7^{β} frequency components, $f_2 + f_5$ and $f_3 + f_4$.

References for Chapter 3:

1. K. Yoshii, J. K. Anthony, and M. Katsuragawa, Light: Sci. Appl. **2,** e58 (2013).
2. K. Yoshii, Y. Nakamura, K. Hagihara and M. Katsuragawa, *CLEO/QELS 2014*, OSA Technical Digest (online) (Optical Society of America, 2014), paper FTh1D.5.

Chapter 4

Experimental results

In this chapter, the experimental results from the system described in Chapter 3 are presented. First, the locking accuracy of the master laser to a reference cavity by using Pound-Drever-Hall technique is presented. Then, the evaluation of the phase-locking performance (phase-lock loop range, phase fluctuations and frequency stability) is explained. The measured beam quality and the spectral power of each generated harmonics are also explained. Finally, the spectral phase coherence among the five harmonics is confirmed by measuring the interference between the sum-frequencies of the harmonics.

4.1 Frequency stability of master laser

This section clarifies the accuracy of the frequency stabilization of master laser by using the PDH technique (described in Section 3.3). The error signal of the master laser (801nm ECDL) at 10 Hz frequency sweep and locked condition by PDH technique using a reference cavity with finesse of 2000 is shown in Fig. 4.1. By using these results, the accuracy of the PDH locking system was clarified.

At the frequency sweep condition, the peak-to-peak value of the error signal near resonance is 1.0 [V]. In the locking condition, the error signal fluctuation is around 60 [mV]. Here, the cavity length is 60 [mm]. The FWHM value of the cavity longitudinal mode Δν is calculated as follows:

$$\Delta\nu = \frac{FSR}{Finesse} = \frac{\frac{c}{2 \times 60mm}}{2000} \approx 1.3\ [MHz]$$

These peak-to-peak value of the error signal in frequency sweeping condition, fluctuation width of the error signal in locking condition, Δν and the locking accuracy of the oscillating frequency are related as follows;

Peak-to-peak value : fluctuation width = Δν : locking accuracy

Therefore, the locking accuracy is,

$$\begin{aligned}\text{Locking accuracy} &= \frac{\text{fluctuation width}}{\text{peak} - \text{to} - \text{peak value}} \times \Delta\nu \\ &= \frac{60\ [mV]}{1.0[V]} \times 1.3\ [MHz] \\ &= 78\ [\text{kHz}]\end{aligned}$$

This frequency stability of the master laser is transferred to all the five generated harmonics through optical frequency division process and QPM nonlinear mixing processes. This level of accuracy might be sufficient for some applications that are not crucially depend on the absolute frequency stability such as AOW

generation. However, for high-precision applications, it is necessary to lock the system to a frequency standard.

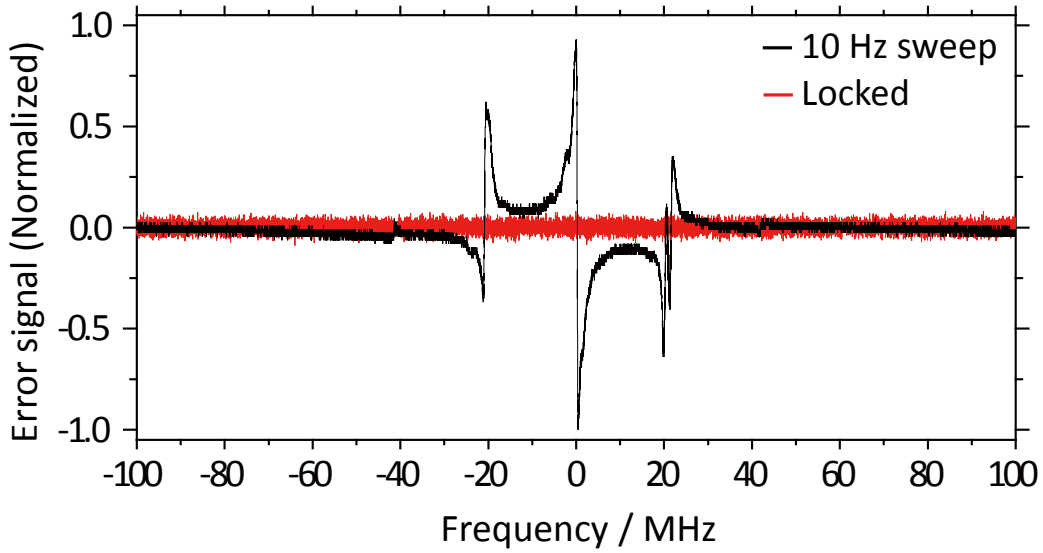

Fig. 4.1: Error signal of the master laser (801nm) at 10 Hz frequency sweep (black line) and locked condition (red line) in PDH locking process by using an optical cavity with finesse = 2000.

4.2 Phase-locking stability via divide - by - three optical frequency divider

This section explains the results from the experiment described in Section 3.4. The performance of the divide-by-three optical frequency divider is evaluated based on the phase-locked loop range, phase fluctuations and frequency fluctuations of the system.

Phase-locked loop range

Phase-locked loop (PLL) range is the frequency range where the PLL circuit can achieve and stay in locking condition. Figure 4.2 shows the frequency spectrum of the beat signal obtained from the divide-by-three optical frequency divider without phase locking (gray), and with phase locking (black). As clearly seen here, when the locking loop was operated, a very sharp peak of central carrier appeared at exactly 95 MHz (expected beat frequency value) with residual noise sideband peaks at a frequency distance of 1.2 MHz. This is called the PLL range. This range implies that 84% of the broad beat spectrum in the unlocked case was pulled into the carrier beat frequency at 95 MHz. Thus the carrier beat frequency power became 25 dB greater than the residual noise sideband peaks. The spectral width of the sharp peak of central carrier supposed to indicate the frequency stability of the beat signal, but the resolution of the spectrum analyzer used to measure this data is limited to 1 kHz (Sweep time: 12.9 sec). Therefore, the beat frequency stability was evaluated by using a frequency counter (data will be explained next).

These results show that the divide-by-three optical frequency division i.e., the locking of f_1, f_2 and f_3 at the exact integer ratio of 1 : 2 : 3, was achieved.

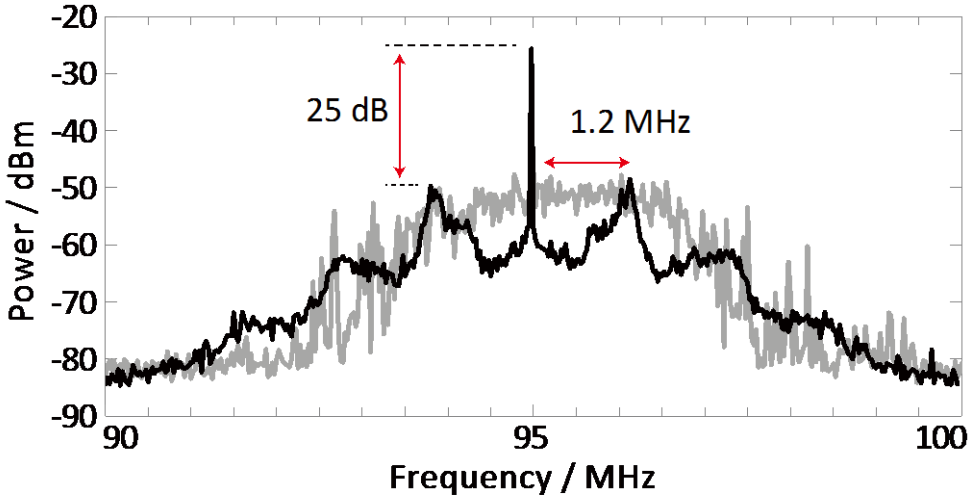

Fig. 4.2: Frequency spectrum of the beat signal without phase locking (gray) and after phase locking (black).

Phase fluctuations

To evaluate the precision of this phase-locking condition, the phase fluctuations of the beat signal was measured by using the error signal that was proportional to the phase deviations of the beat signal from the RF frequency standard. The measured phase fluctuations are presented as a function of time in Fig. 4.3. From the result, the mean-square (MS) value was calculated to be 0.096 rad^2, which is shown as root-mean-square (RMS) value in Fig. 4.3. MS value indicates that the power concentration at the exact harmonic frequency is 91% [1], which is consistent with the observed beat spectrum. This phase locking was maintained stably for at least 30 minutes. The 0.3 rad fluctuation corresponds to ~1/20 of 2π, which is sufficient precision for various practical applications.

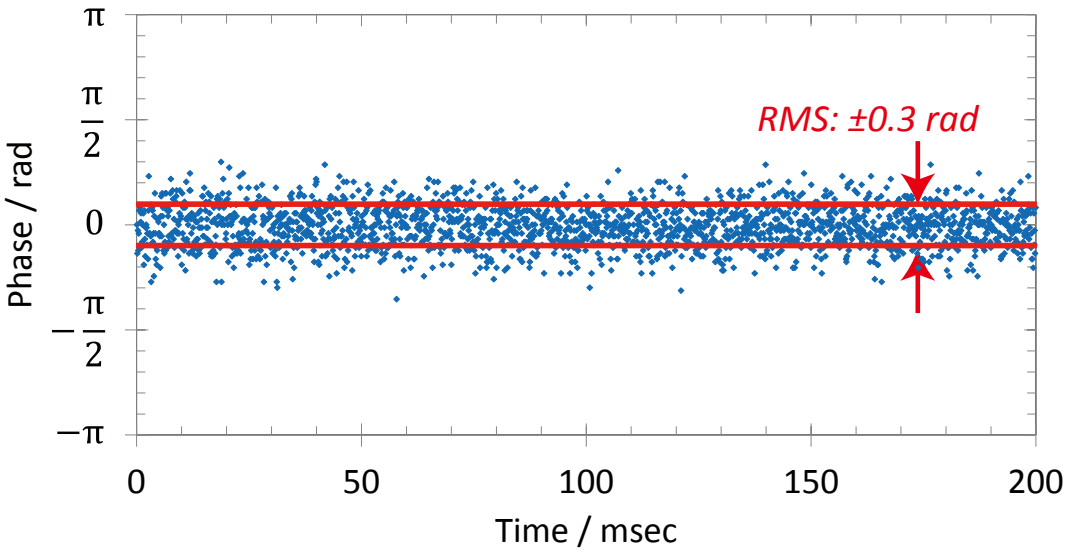

Fig. 4.3: Phase fluctuations of the beat signal.

Frequency fluctuations

In addition to the evaluation of phase fluctuations during phase-locking, the frequency stability of the optical frequency divider was measured to show that the accuracy is reliable. Figure 4.4 shows the Allan deviation of the beat frequency noise relative to the expected value of 1201 nm frequency (249.489696681803 THz). The beat frequency was measured by using a frequency counter with 1 sec counting gate time. The Allan deviation of the beat frequency noise is 5 x10^{-19} in an average time period of 100 sec, which shows that the frequency stability of f_1, f_2 and f_3 is reliable.

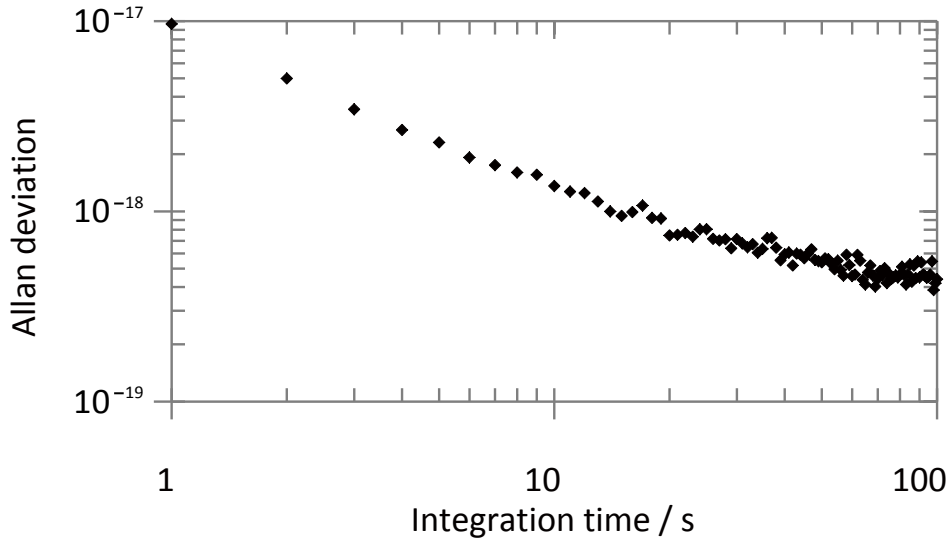

Fig. 4.4: Allan deviation of the beat frequency noise relative to the 1201 nm frequency.

Based on these results, it is clear that the divide-by-three optical frequency divider has succeeded in generating and phase-locking three harmonics (f_1: 2403 nm, f_2: 1201 nm and f_3: 2801 nm) with high phase stability (±0.3 rad phase fluctuations) at a frequency ratio of exactly 1:2:3. In the next section, the generation of a total of five harmonics by the sum frequencies of these three phase-locked harmonics is presented and the characteristics are clarified.

4.3 The generated five harmonics and their characteristics

This section shows the results from the experiment described in Section 3.5. The characteristics of the generated five harmonics are clarified by evaluating the beam quality and spectral power of each harmonic.

Beam quality

Figures 4.5 a, and b show photographs of the five harmonics (except f_1: 2403 nm) obtained from the high harmonics generator, which were taken with a CCD camera (a) before and (b) after we dispersed the beam at the output of WG-PPLN4 with a prism onto a white screen. As seen in the figure, all five harmonics were generated coaxially with a Gaussian-like round beam profile.

Fig. 4.5: Photos of the five generated phase-locked harmonics, a, before b, after dispersal of the harmonic beam with a prism. The 2403-nm radiation is shown by a solid white circle.

The degree of the beam profile variation from the perfect Gaussian beam is quantitatively defined by measuring the M^2 value. M^2 value is a value that indicates how close the laser beam is to being a single mode TEM_{00}, which also indicates how small a beam waist can be focused. The beams were focused with a plano-convex lens of known focal length, and then the characteristics of the beam waist and the divergence were measured by using a Beam Gage beam profiler from Ophir Photonics, except for f_1: 2403 nm beam which was measured by implementing the

knife-edge technique. The obtained data was used to calculate the M^2 value by using the following equation,

$$M^2 = \frac{\theta \pi D}{4\lambda} \tag{4-1}$$

Here, θ is the beam divergence and D is the input beam waist. The results of M^2 value measurement are shown in Fig. 4.6.

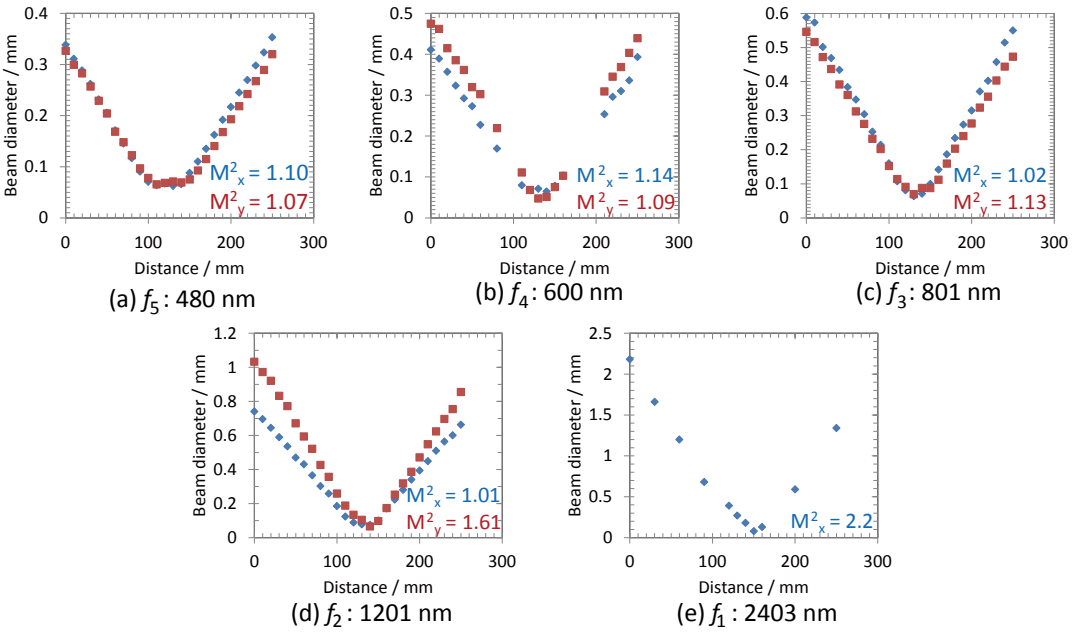

Fig. 4.6: Measured beam waist and divergence of 2403, 1201, 801, 600 and 480 nm radiations at WG-PPLN4 output. Red dots and blue dots indicate y-axis and x-axis measurement, respectively.

The result shows that the shorter wavelengths, f_4: 600 nm and f_5: 480 nm have $M^2<1.2$, which indicates a good single transverse mode. However, the longer wavelengths, f_2: 1201-nm and f_1: 2403-nm have $M^2 \approx 2$. This high value of M^2 is due to the technical difficulty of coupling the longer wavelength through three PPLN waveguides continuously. Nevertheless, the beam quality is still acceptable for further application.

Spectral power

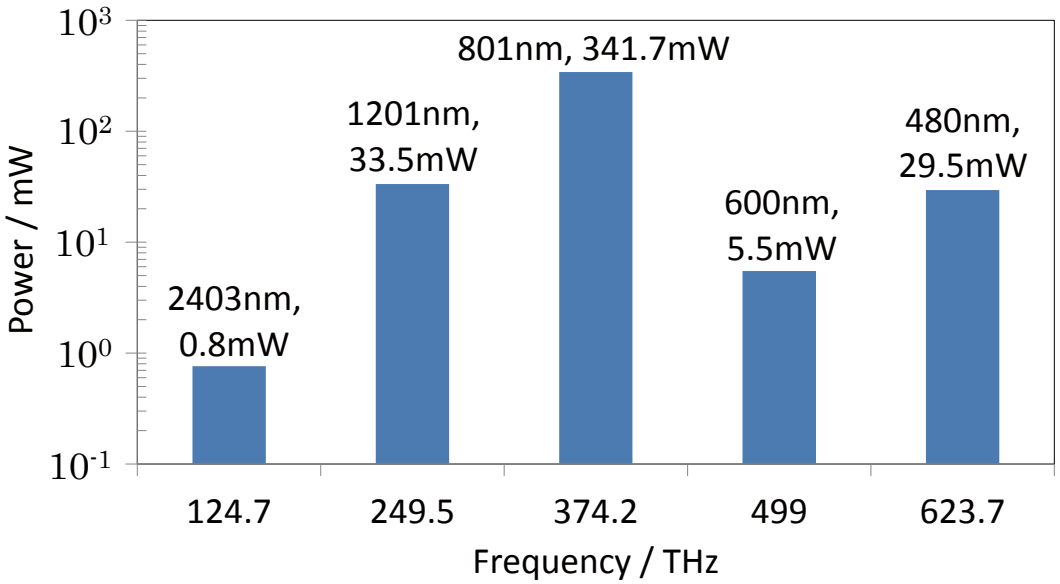

Fig. 4.7 Measured power of generated five phase-locked harmonics.

The power of each generated five phase-locked harmonics was measured at the output of WG-PPLN4 after inserting a bandpass filter for each wavelength. The respective output powers were 0.8, 33.5, 341.7, 5.5 and 29.5 mW for f_1: 2403, f_2: 1201, f_3: 801, f_4: 600 and f_5: 480 nm as shown in Fig. 4.7.

From this result, it can be seen that the power distribution among the spectrum has large differences. The ideal spectral power should be at almost the same value for all the harmonics so that they can be efficiently manipulated for various applications. However, due to the technical difficulty in coupling longer wavelength through multiple waveguides sequentially, spectral power of f_1: 2403 nm radiation decreased in a huge amount. Quantitatively, the amount of losses can be estimated by referring to the coupling efficiency of the harmonics at each PPLN waveguides in Table 2. The converted power of f_4: 600 nm is low because of the low input power of f_1: 2403 nm for the conversion process ($f_1 + f_3 \rightarrow f_4$).

To improve this uneven power distribution, I amplified the output power of the divider laser (f_2: 1201 nm) by adding a commercial semiconductor laser amplifier (BoostaPro, TOPTICA Photonics) to the experimental setup. The divider laser (f_2: 1201 nm) output power was amplified to ~1.2 W. The spectral power measured at

the output of WG-PPLN4 after the amplification is shown in Fig 4.8.

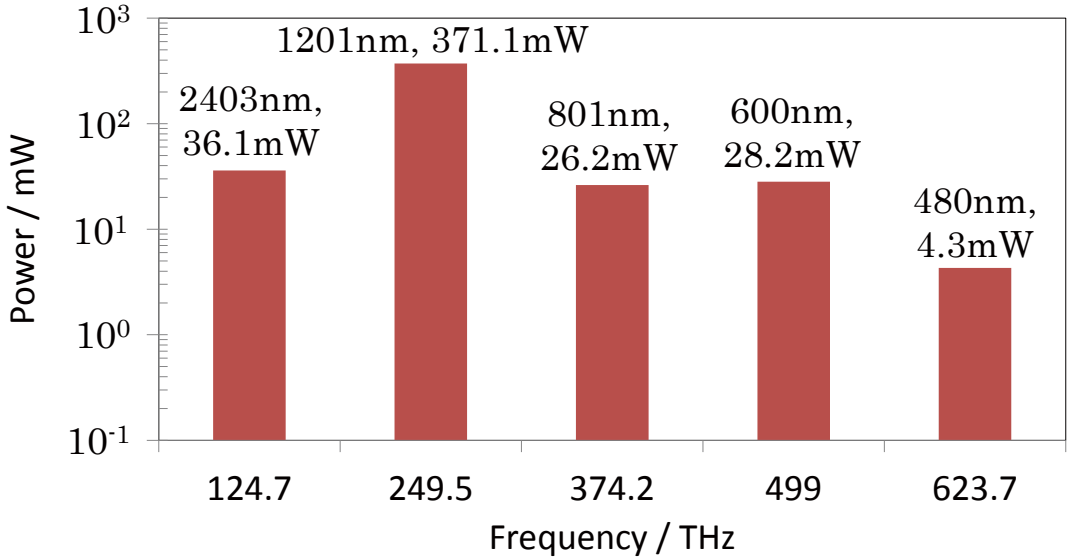

Fig. 4.8: Measured power of generated five phase-locked harmonics after power amplification of divider laser.

The WG-PPLN4 output power of f_1: 2403 nm increased as the initial input power of f_2: 1201 nm used in the conversion process increased to ~500mW. However, this conversion process also resulted in the decrease of spectral power of f_3: 801 nm in order for the energy to be conserved. SFG processes in WG-PPLN 3 ($f_1 + f_3 \rightarrow f_4$) and WG-PPLN4 ($f_2 + f_3 \rightarrow f_5$) also causing the further decrease of f_3: 801 nm due to the same reason. Finally, because of the low power of f_3: 801 nm at the input of WG-PPLN4, the generated f_5: 400 nm becomes lower than the previous result. Nevertheless, the power distribution becomes more reasonable compared to the previous result.

To summarize the results in this section, we have successfully five harmonics were successfully generated with a good single transverse mode quality. To my knowledge, such high quality beam profile has never been reported yet in the generation of coherent broadband light source. Furthermore, the spectral power of each harmonic is in mW level which is very reasonable to be used in further applications.

4.4 Spectral phase analysis

Figure 4.9 shows the interference signal at f_7^{β} aroused with two superimposed f_7^{β} frequency components, $f_2 + f_5$ and $f_3 + f_4$ from the experimental setup described in Section 3.6. The fitting line is the theoretical result from Section 2.5. A sinusoidal-like interference pattern was clearly observed, and almost perfectly fitted with a theoretically predicted curve, which shows that the phase relationship among the high harmonics was well maintained in time and space.

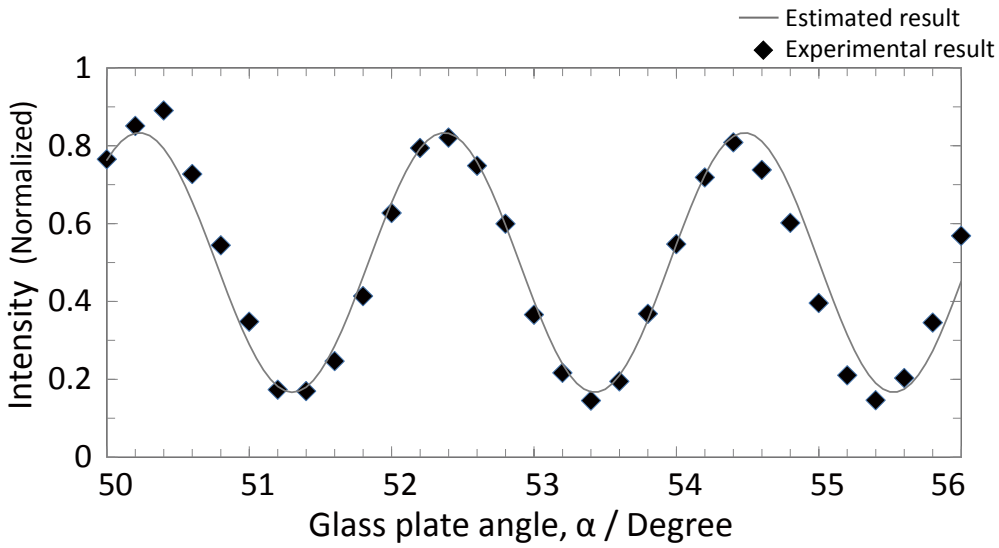

Fig. 4.9: Interference signal aroused with two superimposed f_7^{β} frequency components, $f_2 + f_5$ and $f_3 + f_4$, as a function of the angle α of a glass plate pair inserted in the optical path.

The possible reason for the small difference that occurred in the experimental and theoretical result is due to the surrounding disturbance such as air flow during the measurement being performed. In the experimental setup, the five coaxial harmonics propagated in a free space condition in the lab without an efficient coverage. Furthermore, the measuring process took about 30 minutes to be completed. In such condition and time duration, there is a possibility that the phase

relation between the five harmonics was slightly shifted by the surrounding factor. Therefore, it is recommended for the experimental system to be efficiently covered in the future plan to avoid the surrounding disturbances.

References for Chapter 4:

1. M. Zhu and J. L. Hall, "Stabilization of optical phase/frequency of a laser system: application to a commercial dye laser with an external stabilizer", J. Opt. Soc. Am. B **10**, 802 (1993).

Chapter 5

Conclusions and discussion

I have successfully performed the generation of five phase-locked harmonics in the CW regime with the following features. The limitations are also discussed in this chapter.

Harmonic series of spectrum starting from the fundamental frequency

The spectral components of the generated light are harmonic series of 124.7 THz component, starting from the fundamental (f_1= 124.7 THz) to the 5th harmonic (f_5= 623.7 THz). These frequencies are locked at exact ratio of 1:2:3:4:5. The significant target application that can benefit from this feature is the AOW generation.

Broad-bandwidth

The bandwidth of the generated five harmonics covers from 2403 to 480 nm (124.7 –

623.7 THz). The Fourier transform of such broad bandwidth can be expected to produce ultra-short pulses with pulse duration of ~800 attosec. This could be a key tool for various studies in the attosecond science field.

There is still a potential to increase the bandwidth of the harmonics by performing further frequency mixing process by adding another PPLN waveguide. For example, by performing SHG process of f_3: 801 nm to generate the sixth harmonic f_6: 400 nm. However, due to the technical difficulty of coupling multi-wavelengths into multiple waveguides sequentially, which causes huge power losses and deterioration of beam quality, it was limited to only three waveguides and five harmonics in the experimental system. Therefore, by improving the coupling technique might enable the generation of much higher harmonics.

High phase coherence

The implementation of divide-by-three optical frequency division has successfully phase-locked the five generated harmonics with high stability where the phase fluctuation was only 0.3 rad which corresponds to ~1/20 of 2π. The coaxial layout through the whole system gives the advantage of maintaining the phase coherence in time and space against disturbance. This approach has never been performed by anyone yet. The interference measurement of these five harmonics shows that the phase relation stability can be maintained for at least 30 minutes. With such phase coherence, the manipulation of phase and amplitude of the harmonics can be expected to produce reliable arbitrary optical waveforms in the CW regime.

However, in a long term there is still a possibility for a small phase shift to occur due to surrounding disturbance. Therefore, it is necessary to put the whole system in a confined space to avoid surround disturbance such as air flow.

Extremely wide frequency spacing

The frequency spacing of the generated harmonics is 124.7 THz, which was determined by the frequency difference of the master and the frequency laser. The spacing between the harmonics determines the repetition rate of the pulses that are

Fourier transformed from the harmonics. With a repetition rate of 124.7 THz, the pulse to pulse interval will be around 8 fsec. Ultrashort pulses with high repetition rate could be very useful in the optical communications field. Furthermore, the frequency spacing is important in order to resolve each mode of a frequency comb, where generally a repetition rate of more than 10 GHz is necessary.

Reliable frequency stability

The harmonics are locked at exact ratio of 1:2:3:4:5 with high stability which was indicated by the Allan deviation of the beat frequency noise (5 $x10^{-19}$ in an average time period of 100 sec). However, the absolute frequency fluctuation is 78 kHz (based on stability of PDH locking) which is tolerable for some applications that does not require high precision.

The absolute frequency accuracy can be further improved by locking the system to a frequency standard. With the ultra-high precision from the frequency standard, each of the harmonic can be used as a high accuracy single frequency source.

Practical spectral power

The measured power of the fundamental and the harmonics up to the 5^{th} harmonic was 36.1, 371.1, 26.2, 28.2 and 4.3 mW, respectively. The spectral power hugely depends on the waveguide coupling efficiency and nonlinear conversion efficiency. The obtained spectral power level allows the harmonics to be efficiently manipulated for wider applications. Each of the harmonic can also be directly used as a single frequency laser source.

With all these features, the generated frequency comb is definitely a new achievement in the development of CW light source. Even though the specific target application is not clear yet, there will always be new things to explore. Some of the potentials are mentioned in Chapter 6.

Chapter 6

Future prospects

Generation of arbitrary optical waveforms and ultrashort pulses in the continuous wave regime:

The generation of arbitrary optical waveforms (AOWs) in the CW regime is a huge step towards realizing AOW generator that can produce electric field waveforms in a time scale of few femtoseconds and attosecond. Until now, the generation of practical AOWs in the CW regime is not yet achieved due to the limitation of optical source. The generated light source in this dissertation has a huge potential towards this application. With the advantages of being generated coaxially and exhibited high phase coherence with each other in time and space, they can be efficiently and robustly applied for AOW synthesis in the time domain, including the generation of ultrashort pulse waveform (1.8-fsec pulse duration) [1, 2] in the CW regime. This achievement can be the key technology to open doors to new studies in the atomic world. Furthermore, the ultrashort pulses can be very useful in the ultrafast lightwave communication and attoscience technology.

High precision tunable single frequency lasers:

By locking the system to a frequency standard, the generated five harmonics can be used as ultrahigh-precision single-frequency tunable lasers in the frequency domain. Each of them can be useful for ultra-high precision metrology.

Vibrational Raman sidebands in continuous-wave regime:

I note that the frequency spacing of the produced harmonics exactly matches the vibrational Raman transition in gaseous para-hydrogen. Therefore, they can be used to generate high order stimulated Raman scattering [3-5] which can extend the harmonics wavelength range to the extreme region (mid infrared to vacuum ultraviolet). The employment of a high finesse cavity or a hollow-core photonic crystal fiber (HC-PCF) to confine the gaseous para-hydrogen can increase the gas-matters interaction which will increase the efficiency of Raman sidebands generation. Figure 6.1 shows the schematic illustration of ultra-broad bandwidth optical frequency comb with frequency spacing of 125 THz and its potential applications.

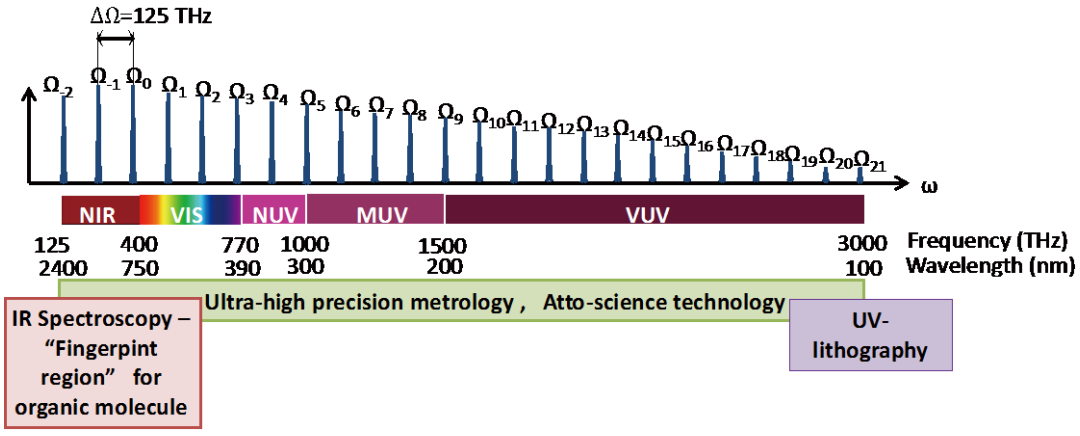

Fig. 6.1: Illustration of ultra-broad bandwidth optical frequency comb with frequency spacing of 125 THz and its potential applications.

References for Chapter 6:

1. K. Yoshii, J. K. Anthony, and M. Katsuragawa, “The simplest route to generating a train of attosecond pulses”, Light: Sci. Appl. 2, e58 (2013).
2. K. Yoshii, Y. Nakamura, K. Hagihara and M. Katsuragawa, “Generation of a Train of Ultrashort Pulses by Simply Inserting Transparent Plates on the Optical Path”, CLEO/QELS 2014, OSA Technical Digest (online) (Optical Society of America, 2014), paper FTh1D.5.
3. S. E. Harris, and A. V. Sokolov, “Broadband spectral generation with refractive index control”, Phys Rev. A 55, R4019 (1997).
4. A. V. Sokolov, D. R. Walker, D. D. Yavuz, G. Y.Yin, and S. E. Harris, “Raman Generation by Phased and Antiphased Molecular States”, Phys. Rev. Lett. 85, 562 (2000).
5. J. Q. Liang, M. Katsuragawa., Fam L. K., and K. Hakuta, “Sideband Generation Using Strongly Driven Raman Coherence in Solid Hydrogen”, Phys. Rev. Lett. 85, 2474 (2000).

APPENDIX A

Properties of the PPLN Waveguide Chips

These are the properties of the total of four PPLN waveguide chips [Courtesy from *NTT Electronics*] used in this dissertation.

Group	QPM-pitch (μm)	WG	WG 厚 (μm)	WG 幅 (μm)	整合温度 予測(℃)	外観検査
G1	20.22	WG1	10.0	12.3	77	OK
		WG2		11.3	59	OK
G2	20.26	WG1		12.3	67	OK
		WG2		11.3	48	OK
G3	20.30	WG1		12.3	57	OK
		WG2		11.3	38	OK
G4	20.34	WG1		12.3	46	OK
		WG2		11.3	28	OK
G5	20.38	WG1		12.3	36	OK
		WG2		11.3	18	OK
G6	20.42	WG1		12.3	26	OK
		WG2		11.3	8	OK

Figure A1. Properties of WG-PPLN1 chip.

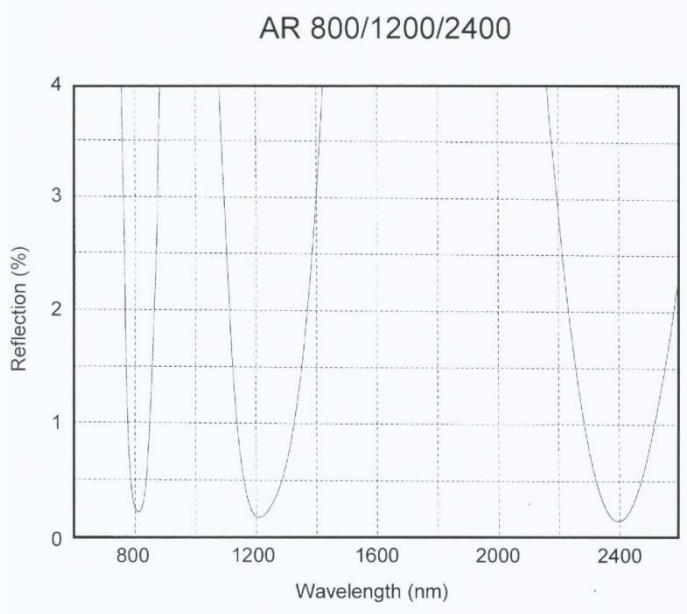

Figure A2. AR coating for WG-PPLN1 chip

S/N:3071295 (ZN132-33-1718) 48mmL 〈2403 → 1201〉

Group	QPM-pitch (μm)	WG	WG厚 (μm)	WG幅 (μm)	整合温度 予測(℃)	外観検査 [キズ・欠け]
G1	31.30	WG1	10.0	11.6	74	OK
		WG2		11.9	78	OK
G2	31.34	WG1		11.6	68	OK
		WG2		11.9	70	OK
G3	31.38	WG1		11.6	61	OK
		WG2		11.9	64	OK
G4	31.42	WG1		11.6	55	OK
		WG2		11.9	58	OK
G5	31.46	WG1		11.6	48	OK
		WG2		11.9	51	OK
G6	31.50	WG1		11.6	41	OK
		WG2		11.9	44	OK

Figure A3. Properties of WG-PPLN2 chip

S/N:3071296 (ZN132-31-2122) 34mmL 〈801 + 2403 -> 600〉

Group	QPM-pitch (μm)	WG	WG厚 (μm)	WG幅 (μm)	整合温度予測(℃)	外観検査
G1	11.63	WG1	10.0	11.2	58	OK
		WG2		11.7	63	OK
G2	11.65	WG1		11.2	50	OK
		WG2		11.7	54	OK
G3	11.67	WG1		11.2	41	右端面△
		WG2		11.7	-	×
G4	11.69	WG1		11.2	34	OK
		WG2		11.7	37	OK
G5	11.71	WG1		11.2	24	OK
		WG2		11.7	28	OK
G6	11.73	WG1		11.2	16	OK
		WG2		11.7	19	OK

Figure A4. Properties of WG-PPLN3 chip

S/N:無し (ZN132-34-0506L) 23mmL 〈801 + 1201 -> 480〉

Group	QPM-pitch (μm)	WG	WG厚 (μm)	WG幅 (μm)	整合温度予測(℃)	外観検査
G1	11.63	WG1	7.3	8.1	61	OK
		WG2		7.8	58	OK
G2	11.65	WG1		8.1	50	OK
		WG2		7.8	47	OK
G3	11.67	WG1		8.1	40	OK
		WG2		7.8	36	OK
G4	11.69	WG1		8.1	31	OK
		WG2		7.8	28	OK
G5	11.71	WG1		8.1	21	OK
		WG2		7.8	16	OK
G6	11.73	WG1		8.1	10	OK
		WG2		7.8	6	OK

Figure A4. Properties of WG-PPLN4 chip

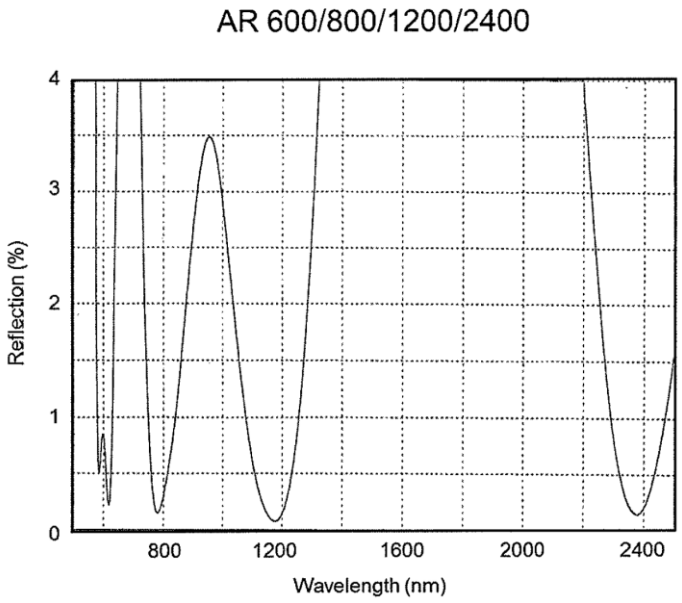

Figure A5. AR coating for WG-PPLN2, WG-PPLN 3, WG-PPLN 4 chips

APPENDIX B

Tapered amplifier setup for master laser

In this experimental system, two tapered amplifiers (TA) are used to amplify the master laser power. The first TA (TA-0785-1000-DHP(F), M2K LASER) amplifies the 801-nm radiation from the ECDL and the second TA (EYP-TPA-0795-02000-4006-CMT04-0000, Eagleyard Photonics) further amplifies the output power from the first TA. Figure B1 shows the layout of the TA system. Several cylindrical lenses are necessary for optimizing the coupling of the beam from free space to optical fiber through a pigtailed aspheric lens fiber collimator.

In this experiment, the seed power of TA1 from the 801-nm ECDL is ~16 mW. The current of TA1 was set at ~1500 mA to give an output power of ~50 mW at TA2 input. Here, the coupling efficiency of TA1 output beam into the single-mode fiber through aspheric lens collimator was ~50%. The current of TA2 was set at ~2700 mA to give an output power of ~1.8 W. The coupling efficiency of TA2 output beam into single-mode fiber through a pigtailed aspheric lens fiber collimator was ~ 55%. Thus, the 801-nm radiation power sent towards WG-PPLN1 was ~1 W.

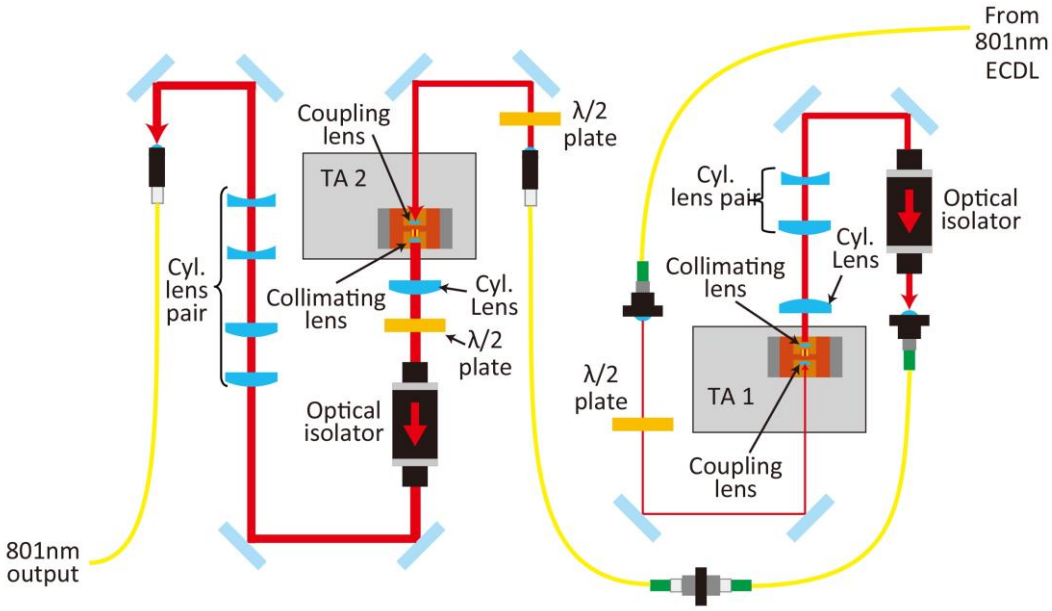

Fig. B1: Layout of the tapered amplifier system. TA: tapered amplifier, Cyl. lens: cylindrical lens.

APPENDIX C

Acousto-optic modulator (AOM) for frequency modulation

Acousto-optic effect is a phenomenon where a light is diffracted and modulated when it propagates through a transparent medium in which the refractive index is changed by the presence of sound waves in that medium. This effect results in modulation of direction, intensity and frequency of the light. The transparent medium that is used to modulate a light by using the acousto-optic effect is called the acousto-optic modulator (AOM).

In this experiment, an AOM from Brimrose Corporation [TEF-110-60-800] is utilized to give a 95 MHz frequency shift to laser frequencies of the slave laser that generates a beat signal for phase locking. The frequency shift is to prevent the beat signal from becoming a DC signal during the phase-locking process.

Figure C1 shows the layout of the actual AOM system for this study. The f_1: 2403nm and f_2: 1201nm components are from the WG-PPLN1 output which are segregated partially from the main line for the phase-locking process.

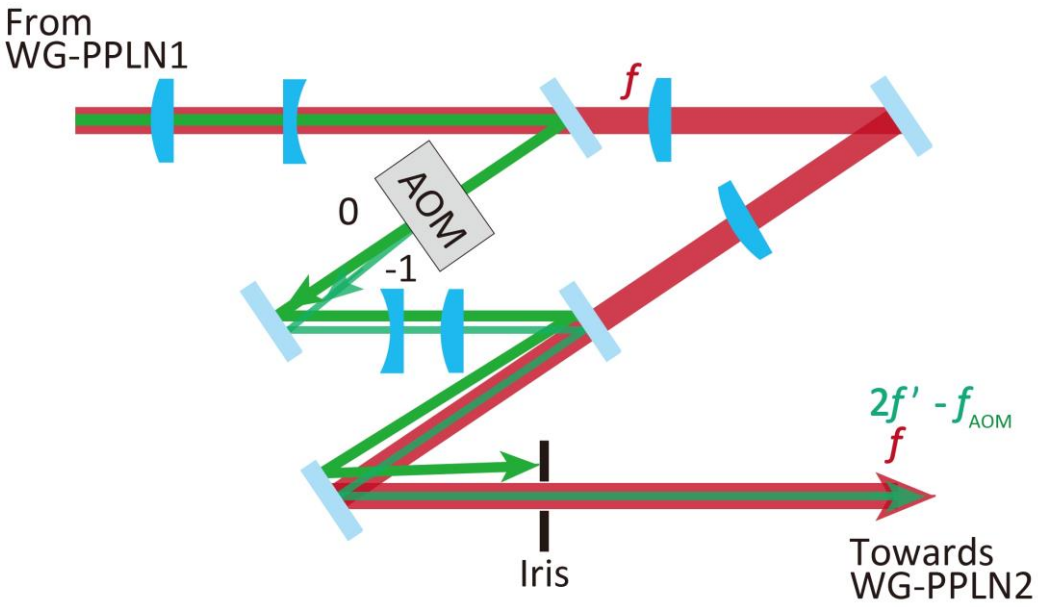

Fig.C1: Layout of the actual AOM setup.

List of Publications, Conference Presentations and Awards

Journal Publications

1) **Nurul Sheeda Suhaimi,** Chiaki Ohae, Trivikramarao Gavara, Ken'ichi Nakagawa, Feng Lei Hong and Masayuki Katsuragawa, "Generation of five phase-locked harmonics by implementing a divide-by-three optical frequency divider", Optics Letters Vol. 40, Issue 24, pp. 5802-5805 (2015).

2) Chiaki Ohae, **Nurul Sheeda Suhaimi**, Trivikramarao Gvara, Ken'ichi Nakagawa, Feng-Lei Hong , Masayuki Katsuragawa, "Frequency division in the optical frequency region and generation of phase-locked high harmonics", Laser Society of Japan, The Review of Laser Engineering, Vol. 43, No. 8, (2015).

International Conferences

1) C. Ohae, S. **Nurul Sheeda Suhaimi**, K. Nakagawa, F. L. Hong and M. Katsuragawa: "Generation of broad phase-locked harmonics", 24th International Laser Physics Workshop (LPHYS'15), Shanghai Institute of Optics and Fine Mechanics, the Chinese Academy of Sciences, Shanghai, China, August 21–25, (2015). ***Invited Paper***

2) **Nurul Sheeda Suhaimi**, C. Ohae, G. Trivikramarao, K. Yoshii, and M. Katsuragawa: "Optical frequency divider and its application in ultra-broadband Raman comb", The second international workshop MIPT (Moscow, Russia) – UEC (Tokyo, Japan): atomic, molecular and optical physics. UEC, Tokyo, Japan, 16-21, October (2014).

4) K. Yoshii, **Nurul Sheeda Suhaimi**, M. Katsuragawa: "Attosecond Temporal Shape Manipulation by Arbitrarily Designing Spectral Phases", CLEO-PR & OECC/PS 2013: The 10th Conference on Lasers and Electro-Optics, Pacific Rim and 18th Optoelectronics and Communications Conference / Photonics in Switching 2013, Attosecond Physics II, TuB4-2, Kyoto International Conference Center, Kyoto, Japan, 30 June – 4 July (2013).

3) **Nurul Sheeda Suhaimi**, M. Katsuragawa: "Ultrabroadband Raman Frequency Comb

with absolute frequency control", The first international workshop MIPT (Moscow, Russia) – UEC (Tokyo, Japan): atomic, molecular and optical physics. MIPT, Moscow, Russia, 30, October – 1, November (2013).

5) **Nurul Sheeda Suhaimi**, Kazumichi Yoshii, Takayuki Suzuki, Kentaro Shiraga, Masaki Arakawa, Feng-Lei Hong and Masayuki Katsuragawa : "Raman Comb With An accuracy Transferred from An Absolute Frequency" , International Workshop on Laser Science (IWLS), (The university of Electro-communications) Chofu, Tokyo, 5-6, October, 2012.

Awards

1) Best Paper Presentation Award
K. Yoshii, Y. Nakamura, K. Hagiwara , **Nurul Sheeda Suhaimi** , and M. Katsuragawa, "Generation of 1.8fsec pulses train by arbitrary phase manipulation of a discrete broadband spectrum" . The 34th Annual Meeting of The Laser Society of Japan, Kitakyushu International Conference Center, Japan (25 Feb 2014).
"

2) Most Progressing Research Award for poster presentation.
Nurul Sheeda Suhaimi, K. Yoshii, T. Kawashima, T. Ohashi, Y. Sasaki, S. Uetake, K. Shiraga, M. Arakawa, F. –L. Hong and M. Katsuragawa, "Raman Comb with Accuracy Transferred from an Absolute Frequency". The 9th TUAT-UEC Joint Symposium, University of Electro-Communication, Japan (15 Dec 2012).